Published for SISSA by Springer

Received: April 20, 2022
Accepted: May 10, 2022
Published: June 13, 2022

Non-factorisable contribution to t-channel single-top production

Christian Brønnum-Hansen,[a] **Kirill Melnikov,**[a] **Jérémie Quarroz,**[a] **Chiara Signorile-Signorile**[a,b] **and Chen-Yu Wang**[a]

[a] *Institute for Theoretical Particle Physics, KIT, Wolfgang-Gaede-Straße 1, Karlsruhe, Germany*
[b] *Institute for Astroparticle Physics, KIT, Hermann-von-Helmholtz-Platz 1, Karlsruhe, Germany*

E-mail: christian.broennum-hansen@kit.edu, kirill.melnikov@kit.edu, jeremie.quarroz@kit.edu, chiara.signorile-signorile@kit.edu, chen-yu.wang@kit.edu

Abstract: We compute the non-factorisable $\mathcal{O}(\alpha_s^2)$ corrections to t-channel single-top quark production at the LHC. These peculiar corrections arise because of interactions between the heavy- and the light-quark lines and appear for the very first time at next-to-next-to-leading order in perturbative QCD. We find that the non-factorisable corrections change the single-top production cross section and the relevant kinematic distributions in this process by about half a percent.

Keywords: Higher-Order Perturbative Calculations, Top Quark, Scattering Amplitudes

ArXiv ePrint: 2204.05770

https://doi.org/10.1007/JHEP06(2022)061

JHEP06(2022)061

Contents

JHEP06(2022)061

1 Introduction

Studies of top quarks are important for the exploration of the Standard Model (SM) and in searches for its extensions. With a mass of more than 170 GeV, the top quark is the heaviest elementary particle of the SM and has an exceptionally strong coupling to the Higgs boson. These special features of top quarks make it plausible that they play a particular role in the underlying mechanism of electroweak symmetry breaking and may have significant couplings to heavy New Physics.

The large top-quark mass is the reason behind its short lifetime which, in fact, is so short that, once produced, top quarks decay before hadronising into mesons and baryons.

This has many interesting consequences including the fact that the information about top-quark polarisation is passed to its decay products offering an opportunity to study this aspect of QCD without non-perturbative contamination.

At the LHC, top quarks are mainly produced in pairs via strong interactions. Theoretical predictions for $t\bar{t}$ pair production are very advanced and include next-to-leading-order (NLO) QCD [1] and electroweak corrections [2], soft gluon resummation [3–7], and total and fully differential next-to-next-to-leading-order (NNLO) QCD corrections [8–11] in the narrow-width approximation.

Top quarks can also be produced via electroweak interactions; this mechanism is referred to as *single-top production*. Interestingly, rates for single-top production at the LHC are quite significant. In fact, the single-top quark production cross section is smaller than the $t\bar{t}$ production cross section by only about a factor of four. However, since the $pp \to t\bar{t}$ cross section at the LHC is large, of the order of a nanobarn, rates for single-top production turn out to be very high as well. As a result, there is a well-developed experimental program for studying single-top production at the LHC that focuses on inferring information about the top-quark width [12], mass [13] and polarisation [14], as well as using this process to constrain possible anomalous couplings in the tWb vertex [15–18]. Studies of single-top production are also used to constrain the CKM matrix element V_{tb}, which has been measured both at the Tevatron [19] and at the LHC [20]. Finally, single-top production can be used to provide interesting probes of parton distribution functions (PDFs). For example, comparison of single-top and single-anti-top production cross sections can be used to constrain ratios of up- and down-quark distribution functions at fairly large values of Bjorken x [21–23].

Single top quarks are produced in hadron collisions in three distinct ways that are conventionally referred to as channels. The t-channel production refers to a process where a W boson is exchanged between two quark lines and a top quark is produced on one of them as the result of the flavour-changing tWb interaction. The s-channel production refers to a process where a virtual W boson is first created in the collisions of light quarks and later decays into a top quark and an anti-bottom quark. The associated production refers to a process where an off-shell bottom quark is produced and then decays into a top quark and a W boson.

Among the three channels, t-channel production is responsible for about 70% of the single-top production cross section. Because of that, this contribution has been carefully scrutinised in the Standard Model. In particular, NLO QCD and NNLO QCD corrections to t-channel single-top production were computed in refs. [24–29] and refs. [30–33], respectively. Results for soft gluon resummation are known to next-to-leading-logarithmic accuracy [34]. In ref. [35] NLO effects of both QCD and electroweak origin were computed. Typically, the inclusive cross section for single-top production changes by about 2–3 percent at next-to-leading order[1] and by 1–3 percent at next-to-next-to-leading order. The reason behind the smallness of these corrections is the proximity of single-top production and deep-inelastic scattering processes which means that a bulk of QCD corrections is absorbed into PDFs by

[1]For certain parton distribution functions, the NLO QCD corrections to single-top production cross section can be more significant, see e.g. ref. [33].

JHEP06(2022)061

virtue of the fitting process. This proximity is destroyed if selection cuts are applied to the final state that are not inclusive with respect to QCD radiation. Indeed, once this is done both NLO and NNLO QCD corrections become larger and can reach $\mathcal{O}(10\%)$ in certain kinematic distributions [33].

It is interesting to remark that the above results [30–33] were obtained in the so-called factorisation approximation that neglects the dynamical crosstalk between the two quark lines. This was done for the following reason: although the two incoming or outgoing quarks can interact by exchanging a gluon already at NLO, it is easy to see that such a contribution does not affect the production cross section at this order because of colour conservation. However, such non-factorisable corrections start contributing at NNLO but they are colour-suppressed relative to factorisable contributions. Conversely, it was recently argued [36] that these non-factorisable contributions could be enhanced by a factor π^2 due to the Glauber phase [37, 38], which would compensate for the colour suppression. In fact, explicit computations of non-factorisable corrections performed in ref. [36] for Higgs production in weak boson fusion proved the existence of such an enhancement factor.

The non-factorisable contributions are quite peculiar. Indeed, they are ultraviolet finite and thus do not require any renormalisation. In addition, as we will show later, they are entirely Abelian, at least at NNLO, which implies a remarkable simplification in their infrared structure. Moreover, they do not contain collinear singularities since, in physical gauges, collinear singularities originate from the emission and absorption of a real or virtual gluon by the same on-shell particle and for the non-factorisable corrections this is impossible because of their definition. As a consequence, all infrared divergences that may appear in non-factorisable corrections are of soft origin and, in dimensional regularisation, correspond to at most double poles in the regulator.

We also expect that virtual effects play a more important role in non-factorisable corrections than the real-emission contributions. This is because the enhancement of the non-factorisable corrections by a Glauber phase is a virtual effect that, in principle, does not require scattering to occur and, hence, remains present also at zero momentum transfer where the cross section is the largest. Indeed, no scattering means no real radiation so we expect that real-emission contributions are, naturally, less important.

Very recently, the two-loop non-factorisable contributions to single-top production were computed in ref. [39]. The results of that reference are, however, not complete since two additional contributions — double-real emissions and virtual corrections to the single-real emission — are required to compute infrared-finite cross sections and kinematic distributions. In this paper we complete the calculation of non-factorisable corrections to the single-top production by computing the two remaining NNLO contributions and, for the first time, provide physical results for non-factorisable corrections to this process.

The paper is organised as follows. In section 2 we introduce the notation and describe the set-up of the calculation. We proceed in section 3 with the treatment of the infrared singularities that affect both the real radiation and the virtual corrections. In section 4 we briefly discuss the calculation of the real and virtual amplitudes. Phenomenological results are reported in section 5. We conclude in section 6.

JHEP06(2022)061

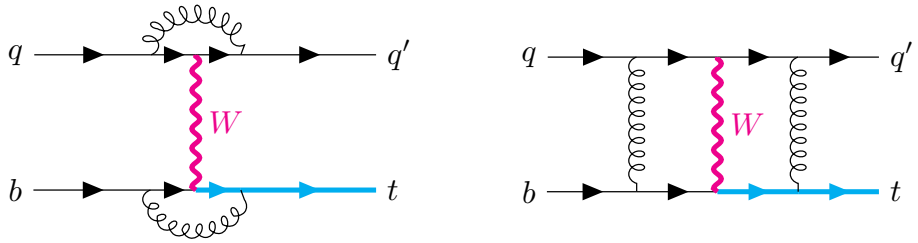

Figure 1. Examples of diagrams contributing to NNLO QCD corrections to single-top production. The diagram on the left is part of the factorisable corrections as the two quark lines interact solely through the exchange of a colourless W boson. On the right, the quark lines are additionally connected by the exchange of two gluons. We classify the latter as a non-factorisable diagram.

2 Colour decomposition of non-factorisable contributions and their singular limits

We mentioned in the introduction that non-factorisable contributions are, effectively, Abelian and that this simplifies their calculation significantly. In this section we explain this point in detail.

2.1 Elastic process

We start with the discussion of the colour decomposition of the relevant partonic processes. Consider single-top production in the t-channel

$$1_q + 2_b \to 3_{q'} + 4_t \,, \tag{2.1}$$

where by i_f we refer to a parton of type f with momentum p_i. Since this process is mediated by a W boson, there is no colour transfer between the two fermion lines. To make this explicit, we use the colour-space formalism[2] and write the Born amplitude as

$$\langle c|\mathcal{M}_0(1_q, 2_b, 3_{q'}, 4_t)\rangle = \delta_{c_3c_1}\delta_{c_4c_2}\, A_0(1_q, 2_b, 3_{q'}, 4_t)\,, \tag{2.2}$$

where A_0 is the colour-stripped amplitude.

In order to compute the NNLO QCD corrections to the process in eq. (2.1), we need the expression for the corresponding one- and two-loop amplitudes. We begin with the former and write it as

$$\langle c|\mathcal{M}_1(1_q, 2_b, 3_{q'}, 4_t)\rangle = \frac{\alpha_s}{2\pi}\left(\delta_{c_3c_1}\delta_{c_4c_2}\, A_1(1_q, 2_b, 3_{q'}, 4_t) + t^a_{c_3c_1}t^a_{c_4c_2}\, B_1(1_q, 2_b, 3_{q'}, 4_t)\right), \tag{2.3}$$

where A_1 describes emissions and absorptions of virtual gluons by the same fermion line and B_1 refers to a one-loop amplitude that describes interactions between light- and heavy-fermion lines. Also, t^a_{ij} are matrix elements of the SU(3) generators and $\alpha_s \equiv \alpha_s(\mu)$ is the renormalised strong coupling constant in the $\overline{\text{MS}}$ scheme (see appendix A for details). It is this last amplitude that is of interest to us, as it contributes to non-factorisable corrections.

[2]The colour-space formalism is reviewed in ref. [40].

JHEP06(2022)061

The B_1 amplitude is ultraviolet-finite but infrared-divergent; the infrared divergence is described by the following formula

$$B_1(1_q, 2_b, 3_{q'}, 4_t) = I_1(\epsilon)\; A_0(1_q, 2_b, 3_{q'}, 4_t) + B_{1,\text{fin}}(1_q, 2_b, 3_{q'}, 4_t)\,, \tag{2.4}$$

where

$$I_1(\epsilon) \equiv I_1(1_q, 2_b, 3_{q'}, 4_t; \epsilon) = \frac{1}{\epsilon}\left[\log\left(\frac{p_1\cdot p_4\; p_2\cdot p_3}{p_1\cdot p_2\; p_3\cdot p_4}\right) + 2\pi i\right]. \tag{2.5}$$

We can write the two-loop amplitude in a similar manner. First, we define the non-factorisable contribution to the amplitude as follows

$$\langle c|\mathcal{M}_2(1_q, 2_b, 3_{q'}, 4_t)\rangle = \left(\frac{\alpha_s}{2\pi}\right)^2 \left(\ldots + \frac{1}{2}\{t^a, t^b\}_{c_3 c_1}\frac{1}{2}\{t^a, t^b\}_{c_4 c_2}\; B_2(1_q, 2_b, 3_{q'}, 4_t)\right), \tag{2.6}$$

where ellipses stand for factorisable contributions as well as contributions that vanish upon interference with the tree-level amplitude, eq. (2.2). The non-factorisable amplitude B_2 is infrared-divergent; these divergences can be written in the following way

$$\begin{aligned} B_2(1_q, 2_b, 3_{q'}, 4_t) = &-\frac{I_1^2(\epsilon)}{2}\; A_0(1_q, 2_b, 3_{q'}, 4_t) + I_1(\epsilon)\; B_1(1_q, 2_b, 3_{q'}, 4_t) \\ &+ B_{2,\text{fin}}(1_q, 2_b, 3_{q'}, 4_t)\,. \end{aligned} \tag{2.7}$$

We stress that the finite contributions to B_2 arise from the two last terms. Hence, to obtain $B_{2,\text{fin}}$ in eq. (2.7), we require the one-loop amplitude B_1 to $\mathcal{O}(\epsilon)$.

To compute the cross section, we need a particular combination of these elastic amplitudes. We require

$$\begin{aligned} &|\mathcal{M}_1(1_q, 2_b, 3_{q'}, 4_t)|^2_{\text{nf}} + 2\text{Re}\left[\mathcal{M}_0^*(1_q, 2_b, 3_{q'}, 4_t)\,\mathcal{M}_2(1_q, 2_b, 3_{q'}, 4_t)\right]_{\text{nf}} \\ &= \frac{N^2-1}{4}\left(\frac{\alpha_s}{2\pi}\right)^2 \Big[-\text{Re}\left[I_1^2(\epsilon)\right]|A_0(1_q, 2_b, 3_{q'}, 4_t)|^2 + |B_1(1_q, 2_b, 3_{q'}, 4_t)|^2 \\ &\qquad + 2\text{Re}\left[I_1(\epsilon)\; A_0^*(1_q, 2_b, 3_{q'}, 4_t)\; B_1(1_q, 2_b, 3_{q'}, 4_t)\right] \\ &\qquad + 2\text{Re}\left[A_0^*(1_q, 2_b, 3_{q'}, 4_t)\; B_{2,\text{fin}}(1_q, 2_b, 3_{q'}, 4_t)\right]\Big], \end{aligned} \tag{2.8}$$

where $N = 3$ is the number of colours. We can now manipulate eq. (2.8) to make all the divergences explicit and expose terms that contribute through $\mathcal{O}(\epsilon^0)$. We obtain

$$\begin{aligned} &|\mathcal{M}_1(1_q, 2_b, 3_{q'}, 4_t)|^2_{\text{nf}} + 2\text{Re}\left[\mathcal{M}_0^*(1_q, 2_b, 3_{q'}, 4_t)\mathcal{M}_2(1_q, 2_b, 3_{q'}, 4_t)\right]_{\text{nf}} \\ &= \frac{N^2-1}{4}\left(\frac{\alpha_s}{2\pi}\right)^2 \Big[2\left(\text{Re}\left[I_1(\epsilon)\right]\right)^2|A_0(1_q, 2_b, 3_{q'}, 4_t)|^2 + |B_{1,\text{fin}}(1_q, 2_b, 3_{q'}, 4_t)|^2 \\ &\qquad + 4\text{Re}\left[I_1(\epsilon)\right]\text{Re}\left[A_0^*(1_q, 2_b, 3_{q'}, 4_t)\; B_{1,\text{fin}}(1_q, 2_b, 3_{q'}, 4_t)\right] \\ &\qquad + 2\text{Re}\left[A_0^*(1_q, 2_b, 3_{q'}, 4_t)\; B_{2,\text{fin}}(1_q, 2_b, 3_{q'}, 4_t)\right]\Big]. \end{aligned} \tag{2.9}$$

It follows that the first term contains a $1/\epsilon^2$ divergence, the third a $1/\epsilon$ divergence and the remaining two terms are finite.

JHEP06(2022)061

2.2 Single-real emission contributions

Similarly, the tree-level amplitude for the single-emission process

$$1_q + 2_b \to 3_{q'} + 4_t + 5_g \,, \tag{2.10}$$

reads

$$\begin{aligned}\langle c|\mathcal{M}_0(1_q,2_b,3_{q'},4_t;5_g)\rangle = \; g_{s,b}\Big[&t^{c_5}_{c_3c_1}\delta_{c_4c_2}A_0^L(1_q,2_b,3_{q'},4_t;5_g)\\ &+ t^{c_5}_{c_4c_2}\delta_{c_3c_1}A_0^H(1_q,2_b,3_{q'},4_t;5_g)\Big],\end{aligned} \tag{2.11}$$

where A_0^L and A_0^H are colour-stripped amplitudes that describe gluon emission off the light- and heavy-quark lines respectively. Here and in the following $g_{s,b}$ is the bare coupling constant.[3] The soft limits of these colour-ordered amplitudes are relevant for the construction of subtraction terms. To describe them, we introduce the eikonal current

$$J^\mu(i,j;k) = \frac{p_i^\mu}{p_i\cdot p_k} - \frac{p_j^\mu}{p_j\cdot p_k}\,, \tag{2.12}$$

and its contraction with the polarisation vector of a gluon with momentum k

$$\varepsilon_{k,\mu}J^\mu(i,j;k) = J(i,j;k,\varepsilon_k)\,. \tag{2.13}$$

Then, we write

$$\begin{aligned}S_5\,A_0^L(1_q,2_b,3_{q'},4_t;5_g) &= J(3,1;5,\varepsilon_5)\,A_0(1_q,2_b,3_{q'},4_t)\,,\\ S_5\,A_0^H(1_q,2_b,3_{q'},4_t;5_g) &= J(4,2;5,\varepsilon_5)\,A_0(1_q,2_b,3_{q'},4_t)\,.\end{aligned} \tag{2.14}$$

Here we have introduced the operator S_i, which extracts the leading singular behaviour in the soft limit $p_i \to 0$ of the function it acts upon.

We will also need the one-loop contribution to the amplitude of the process in eq. (2.10). Its colour decomposition reads

$$\begin{aligned}\langle c|\mathcal{M}_1(1_q,2_b,3_{q'},4_t;5_g)\rangle \;= g_{s,b}\left(\frac{\alpha_s}{2\pi}\right)\Big[&t^{c_5}_{c_3c_1}\delta_{c_4c_2}\,A_1^L(5_g) + t^{c_5}_{c_4c_2}\delta_{c_3c_1}\,A_1^H(5_g)\\ &+\frac{1}{2}\,\{t^a,t^{c_5}\}_{c_3c_1}\,t^a_{c_4c_2}\,B_1^{sL}(5_g) + \frac{1}{2}\,[t^a,t^{c_5}]_{c_3c_1}\,t^a_{c_4c_2}\,B_1^{aL}(5_g)\\ &+\frac{1}{2}\,\{t^a,t^{c_5}\}_{c_4c_2}\,t^a_{c_3c_1}\,B_1^{sH}(5_g) + \frac{1}{2}\,[t^a,t^{c_5}]_{c_4c_2}\,t^a_{c_3c_1}\,B_1^{aH}(5_g)\Big].\end{aligned} \tag{2.15}$$

In eq. (2.15) we split the full amplitude into colour-stripped amplitudes that describe emissions by light- and heavy-quark lines separately. For each of the quark lines, we have also split the amplitudes into colour-symmetric and colour-antisymmetric parts, indicated with superscripts s and a respectively. The colour-symmetric ones are purely Abelian and

[3] We stress that in this paper we have used α_s to indicate the renormalised coupling constant and suppressed its dependence on the scale μ, while $g_{s,b}$ is the bare coupling.

JHEP06(2022)061

the colour-antisymmetric ones are sensitive to the non-Abelian nature of QCD, including contributions due to the gluon self-coupling. Note that we have suppressed the dependence of the amplitudes A_1 and B_1 on the quark momenta but kept their dependences on the final-state gluon momentum.

It is now straightforward to contract this amplitude with the tree-level amplitude of the single-emission process given in eq. (2.11). Singling out the non-factorisable contributions, we obtain

$$\begin{aligned} &2\mathrm{Re}\big[\mathcal{M}_0^*(1_q,2_b,3_{q'},4_t;5_g)\mathcal{M}_1(1_q,2_b,3_{q'},4_t;5_g)\big]_{\mathrm{nf}} \\ &\qquad = g_{s,b}^2\,\frac{N^2-1}{4}\left(\frac{\alpha_s}{2\pi}\right)\Big(A_0^{L*}(5_g)\,B_1^{sH}(5_g)+A_0^{H*}(5_g)\,B_1^{sL}(5_g)+\mathrm{c.c.}\Big)\,. \end{aligned} \tag{2.16}$$

It follows from the definition of the colour-stripped amplitudes in eq. (2.15) that non-factorisable contributions are fully determined by Abelian amplitudes.

We are now able to discuss divergences and singular limits of non-factorisable amplitudes. Infrared divergences of symmetric amplitudes $B_1^{sL(H)}$ do not depend on the fact that an additional gluon is emitted and, therefore, can still be described by the factor I_1 shown in eq. (2.5). We find

$$B_1^{sL(H)}(1_q,2_b,3_{q'},4_t;5_g) = I_1(\epsilon)\,A_0^{L(H)}(1_q,2_b,3_{q'},4_t;5_g)+B_{1,\mathrm{fin}}^{sL(H)}(1_q,2_b,3_{q'},4_t;5_g)\,. \tag{2.17}$$

In addition to the infrared-divergent contribution to the one-loop, single-emission amplitude, we require its soft limit. Again, thanks to the Abelian nature of the amplitudes that contribute to non-factorisable corrections, we can write

$$\begin{aligned} S_5\,B_1^{sL}(1_q,2_b,3_{q'},4_t;5_g) &= J(3,1;5,\varepsilon_5)\,B_1(1_q,2_b,3_{q'},4_t)\,,\\ S_5\,B_1^{sH}(1_q,2_b,3_{q'},4_t;5_g) &= J(4,2;5,\varepsilon_5)\,B_1(1_q,2_b,3_{q'},4_t)\,. \end{aligned} \tag{2.18}$$

Hence,

$$\begin{aligned} &S_5\left\{2\mathrm{Re}\left[\mathcal{M}_0^*(1_q,2_b,3_{q'},4_t;5_g)\mathcal{M}_1(1_q,2_b,3_{q'},4_t;5_g)\right]_{\mathrm{nf}}\right\} \\ &= -g_{s,b}^2\,\frac{N^2-1}{2}\left(\frac{\alpha_s}{2\pi}\right)\mathrm{Eik}_{\mathrm{nf}}(1_q,2_b,3_{q'},4_t;5_g)\,2\mathrm{Re}\left[A_0^*(1_q,2_b,3_{q'},4_t)\,B_1(1_q,2_b,3_{q'},4_t)\right]\,, \end{aligned} \tag{2.19}$$

where the eikonal factor reads

$$\mathrm{Eik}_{\mathrm{nf}}(1_q,2_b,3_{q'},4_t;k_g) = J^\mu(3,1;k)J_\mu(4,2;k) = \sum_{\substack{i\in[1,3]\\ j\in[2,4]}}\frac{\lambda_{ij}\,p_i\cdot p_j}{(p_i\cdot p_k)(p_j\cdot p_k)}\,, \tag{2.20}$$

with $\lambda_{ij}=+1$ if both i and j are either incoming or outgoing, and $\lambda_{ij}=-1$ otherwise.

2.3 Double-real emission amplitudes

The double-emission process describes the radiation of two real gluons. We parametrise this process as follows

$$1_q + 2_b \to 3_{q'} + 4_t + 5_g + 6_g\,, \tag{2.21}$$

JHEP06(2022)061

and write the amplitude as

$$\begin{aligned}
&\langle c|\mathcal{M}_0(1_q,2_b,3_{q'},4_t;5_g,6_g)\rangle \\
&\quad= g_{s,b}^2\Bigg[\frac{1}{2}\{t^{c_5},t^{c_6}\}_{c_3c_1}\delta_{c_4c_2}\,A_0^{sL}(5_g,6_g)+\frac{1}{2}[t^{c_5},t^{c_6}]_{c_3c_1}\delta_{c_4c_2}\,A_0^{aL}(5_g,6_g) \\
&\qquad+\frac{1}{2}\{t^{c_5},t^{c_6}\}_{c_4c_2}\delta_{c_3c_1}\,A_0^{sH}(5_g,6_g)+\frac{1}{2}[t^{c_5},t^{c_6}]_{c_4c_2}\delta_{c_3c_1}\,A_0^{aH}(5_g,6_g) \\
&\qquad+t^{c_5}_{c_3c_1}t^{c_6}_{c_4c_2}\,B_0^{5L,6H}(5_g,6_g)+t^{c_6}_{c_3c_1}t^{c_5}_{c_4c_2}\,B_0^{6L,5H}(5_g,6_g)\Bigg].
\end{aligned} \tag{2.22}$$

Similarly to eq. (2.15), we split the full amplitude into amplitudes for emissions by light- and heavy-quark lines. However, there are additional contributions when one gluon is emitted off the light-quark line and the other off the heavy-quark line. Again, the colour-symmetric parts are purely Abelian and the colour-antisymmetric ones are present because of the non-Abelian nature of QCD. Finally, we note that we have suppressed the dependence of the colour-stripped amplitudes on the quark momenta.

It is straightforward to compute the non-factorisable contributions to the square of the double-real emission amplitude shown in eq. (2.22). We account for contributions such that each gluon is emitted and absorbed by a different quark line and find

$$\begin{aligned}
|\mathcal{M}_0(1_q,2_b,3_{q'},4_t;5_g,6_g)|^2_{\rm nf} &= g_{s,b}^4\,\frac{N^2-1}{4} \\
&\times\Big(A_0^{sL}(5_g,6_g)\,A_0^{sH*}(5_g,6_g)+B_0^{5L,6H}(5_g,6_g)\,B_0^{6L,5H*}(5_g,6_g)+\text{c.c.}\Big),
\end{aligned} \tag{2.23}$$

where the sum over colours has been performed and the sum over polarisations of all final-state quarks and gluons is assumed.

It follows from eq. (2.23) that since the non-factorisable contributions depend on particular combinations of colour-stripped amplitudes, they have peculiar properties. First, these contributions only depend on the Abelian parts of the amplitudes. Second, since only interference terms appear in eq. (2.23), there are no collinear singularities in the non-factorisable contributions.

We will need the single-soft limit of the double-real emission amplitude. Considering $p_6\to 0$ as an example, we obtain the following soft limits of the colour-stripped amplitudes

$$\begin{aligned}
S_6\,B_0^{5L,6H}(1_q,2_b,3_{q'},4_t;5_g,6_g) &= J(4,2;6,\varepsilon_6)\;A_0^{L}(1_q,2_b,3_{q'},4_t;5_g)\,,\\
S_6\,B_0^{6L,5H}(1_q,2_b,3_{q'},4_t;5_g,6_g) &= J(3,1;6,\varepsilon_6)\;A_0^{H}(1_q,2_b,3_{q'},4_t;5_g)\,,\\
S_6\,A_0^{sL}(1_q,2_b,3_{q'},4_t;5_g,6_g) &= J(3,1;6,\varepsilon_6)\;A_0^{L}(1_q,2_b,3_{q'},4_t;5_g)\,,\\
S_6\,A_0^{sH}(1_q,2_b,3_{q'},4_t;5_g,6_g) &= J(4,2;6,\varepsilon_6)\;A_0^{H}(1_q,2_b,3_{q'},4_t;5_g)\,.
\end{aligned} \tag{2.24}$$

Hence,

$$\begin{aligned}
S_6\,|\mathcal{M}_0(1_q,2_b,3_{q'},4_t;5_g,6_g)|^2_{\rm nf} &= -g_{s,b}^4\,\frac{N^2-1}{2}\,\mathrm{Eik}_{\rm nf}(1_q,2_b,3_{q'},4_t;6_g) \\
&\times\Big[A_0^{L}(1_q,2_b,3_{q'},4_t;5_g)\,A_0^{H*}(1_q,2_b,3_{q'},4_t;5_g)+\text{c.c.}\Big]\,.
\end{aligned} \tag{2.25}$$

JHEP06(2022)061

We also need the double-soft limits of the colour-stripped amplitudes. We make use of the fact that in an Abelian theory soft limits of amplitudes fully factorise. Therefore, we obtain

$$\begin{aligned}
S_5 S_6\, B_0^{5L,6H}(5_g,6_g) &= J(3,1;5,\varepsilon_5)\; J(4,2;6,\varepsilon_6)\, A_0(1_q,2_b,3_{q'},4_t)\,,\\
S_5 S_6\, B_0^{6L,5H}(5_g,6_g) &= J(3,1;6,\varepsilon_6)\; J(4,2;5,\varepsilon_5)\, A_0(1_q,2_b,3_{q'},4_t)\,,\\
S_5 S_6\, A_0^{sL}(5_g,6_g) &= J(3,1;6,\varepsilon_6)\; J(3,1;5,\varepsilon_5)\, A_0(1_q,2_b,3_{q'},4_t)\,,\\
S_5 S_6\, A_0^{sH}(5_g,6_g) &= J(4,2;6,\varepsilon_6)\; J(4,2;5,\varepsilon_5)\, A_0(1_q,2_b,3_{q'},4_t)\,.
\end{aligned} \tag{2.26}$$

The double-soft limit of the non-factorisable contribution to the amplitude follows immediately. We find

$$\begin{aligned}
S_5 S_6\, |\mathcal{M}_0(1_q,2_b,3_{q'},4_t;5_g,6_g)|^2_{\rm nf} &= g_{s,b}^4\,(N^2-1)\,|A_0(1_q,2_b,3_{q'},4_t)|^2\\
&\quad\times \mathrm{Eik}_{\rm nf}(1_q,2_b,3_{q'},4_t;5_g)\;\mathrm{Eik}_{\rm nf}(1_q,2_b,3_{q'},4_t;6_g)\,.
\end{aligned} \tag{2.27}$$

3 Construction of the subtraction terms

We can use the results of the previous section to extract singularities from non-factorisable contributions to single-top production. For the sake of definiteness, we focus on the total cross section, but the described procedure applies verbatim to any *infrared-safe* observable.

3.1 Double-real cross section

We start by considering the process in eq. (2.21), which we will refer to as the double-real contribution. To describe how the corresponding cross section can be computed, we make use of the notation introduced in ref. [41] and define the function

$$\begin{aligned}
F^{\rm nf}_{\rm LM}\,(1_q,2_b,3_{q'},4_t;5_g,6_g) &= \mathcal{N}\int \mathrm{dLips}_{34}\,(2\pi)^d\,\delta^{(d)}\left(p_1+p_2-\sum_{i=3}^{6}p_i\right)\\
&\quad\times\;|\mathcal{M}_0\,(1_q,2_b,3_{q'},4_t;5_g,6_g)\,|^2_{\rm nf}\,.
\end{aligned} \tag{3.1}$$

Here dLips_{34} is the Lorentz-invariant phase space of the two final state fermions and $\mathcal{N}$ includes spin and colour averaging factors, $\mathcal{N}=1/(4N^2)$. The total cross section can be obtained by integrating over the phase space of the two gluons, 5_g and 6_g, and including the appropriate symmetry factor. We write

$$\begin{aligned}
2s\cdot\sigma^{\rm nf}_{\rm RR} &= \frac{1}{2!}\int [\mathrm{d}p_5]\,[\mathrm{d}p_6]\,F^{\rm nf}_{\rm LM}\,(1_q,2_b,3_{q'},4_t;5_g,6_g)\\
&\equiv \langle F^{\rm nf}_{\rm LM}\,(1_q,2_b,3_{q'},4_t;5_g,6_g)\,\rangle\,,
\end{aligned} \tag{3.2}$$

where $s=2p_1\cdot p_2$ is the partonic centre-of-mass energy squared. The phase space element $[\mathrm{d}p]$ is defined as in ref. [41] and reads

$$[\mathrm{d}p] = \frac{\mathrm{d}^{d-1}p}{(2\pi)^{d-1}2E_p}\,\theta(E_{\rm max}-E_p)\,, \tag{3.3}$$

JHEP06(2022)061

where $E_{\max}$ is a parameter that should be equal to or greater than the maximal energy that a final-state parton can reach according to momentum conservation. In the present paper we use $E_{\max} = \sqrt{s}/2$. The matrix element appearing in eq. (3.1) develops singularities when at least one gluon becomes soft. As we have already mentioned, no collinear divergences affect non-factorisable corrections since they are, essentially, the interference contributions. In order to preserve the fully differential nature of the calculation, we need to regulate and extract soft singularities without integrating over the resolved part of phase space. To do so, we introduce the identity

$$\begin{aligned}\left\langle F^{\rm nf}_{\rm LM}\left(1_q,2_b,3_{q'},4_t;5_g,6_g\right)\right\rangle =& \left\langle S_5 S_6\, F^{\rm nf}_{\rm LM}\left(1_q,2_b,3_{q'},4_t;5_g,6_g\right)\right\rangle \\ &+2\left\langle S_6\left(I-S_5\right) F^{\rm nf}_{\rm LM}\left(1_q,2_b,3_{q'},4_t;5_g,6_g\right)\right\rangle \\ &+\left\langle \left(I-S_5\right)\left(I-S_6\right) F^{\rm nf}_{\rm LM}\left(1_q,2_b,3_{q'},4_t;5_g,6_g\right)\right\rangle .\end{aligned} \tag{3.4}$$

The first term corresponds to the double-soft limit, the second one to the single-soft limit. The last term gives the hard contribution where all singularities are regulated. Note that these terms are symmetric under the exchange of the two gluons due to the factorisation in eq. (2.27) and the integration in eq. (3.1).

The fully regulated term can be computed numerically in four dimensions without further ado. However, we still need to treat the soft-divergent terms. When soft operators act on $F^{\rm nf}_{\rm LM}$ they impact both the squared matrix element and the momentum conserving delta function in its definition. The latter becomes independent of the soft momenta. The single- and double-soft limits of the double-real, non-factorisable matrix elements are given in eqs. (2.25) and (2.27), respectively. In both cases, the matrix element factorises into the universal structure $\mathrm{Eik}_{\rm nf}$, defined in eq. (2.20), and a lower multiplicity matrix element, which does not depend on the soft radiation. We can then integrate over the unresolved momenta without affecting the kinematics of the resolved partons. We perform this integration using dimensional regularisation, i.e. in $d = 4 - 2\epsilon$ dimensions. To present the result of the integration, we find it convenient to define the function

$$g^2_{s,b}\int [\mathrm{d}p_k]\,\mathrm{Eik}_{\rm nf}(1_q,2_b,3_{q'},4_t;k_g) \equiv \frac{\alpha_s}{2\pi}\left(\frac{2E_{\max}}{\mu}\right)^{-2\epsilon} K_{\rm nf}(1_q,2_b,3_{q'},4_t;\epsilon)\,. \tag{3.5}$$

The function $K_{\rm nf}(\epsilon) \equiv K_{\rm nf}(1_q,2_b,3_{q'},4_t;\epsilon)$ can be found in appendix B where it is computed up to $\mathcal{O}(\epsilon^0)$ terms. We now extract the soft divergences and write

$$\begin{aligned}2s\cdot\sigma_{RR} =& \left(\frac{\alpha_s}{2\pi}\right)^2 \frac{N^2-1}{2N^2}\left(\frac{2E_{\max}}{\mu}\right)^{-4\epsilon}\left\langle K^2_{\rm nf}(\epsilon)\, F_{\rm LM}(1_q,2_b,3_{q'},4_t)\right\rangle \\ &-\left(\frac{\alpha_s}{2\pi}\right)\frac{N^2-1}{2}\left(\frac{2E_{\max}}{\mu}\right)^{-2\epsilon}\left\langle K_{\rm nf}(\epsilon)\left(I-S_5\right)\widetilde{F}^{\rm nf}_{\rm LM}(1_q,2_b,3_q,4_t;5_g)\right\rangle \\ &+\left\langle (I-S_5)(I-S_6)\, F^{\rm nf}_{\rm LM}(1_q,2_b,3_{q'},4_t;5_g,6_g)\right\rangle.\end{aligned} \tag{3.6}$$

In the above equation we have introduced a function to describe the tree-level process,

$$F_{\rm LM}\left(1_q,2_b,3_{q'},4_t\right) = \mathcal{N}\int \mathrm{dLips}_{34}\,(2\pi)^d\,\delta^{(d)}(p_1+p_2-p_3-p_4)\left|\mathcal{M}_0\left(1_q,2_b,3_{q'},4_t\right)\right|^2. \tag{3.7}$$

JHEP06(2022)061

We stress that in eq. (3.6) the function $K_{\rm nf}(\epsilon)$ appears inside angular brackets emphasising its dependence on the kinematics of hard particles. We also introduced a non-factorisable, single-gluon emission contribution $\widetilde{F}^{\rm nf}_{\rm LM}$. The tilde stresses that this contribution is defined in terms of colour-stripped amplitudes

$$\begin{aligned}\widetilde{F}^{\rm nf}_{\rm LM}(1_q,2_b,3_q,4_t;5_g) = &\mathcal{N}\int {\rm dLips}_{34}\,(2\pi)^d\,\delta^{(d)}\left(p_1+p_2-\sum_{i=3}^{5}p_i\right)\\ &\times\; g_{s,b}^2\left(A_0^{L*}(1_q,2_b,3_q,4_t;5_g)\,A_0^{H}(1_q,2_b,3_q,4_t;5_g)+{\rm c.c.}\right)\,.\end{aligned} \tag{3.8}$$

This distinction is useful because such interference terms emerge from soft limits of higher-multiplicity amplitudes, but otherwise do not contribute to non-factorisable corrections due to colour conservation.

3.2 Real-virtual cross section

A similar calculation can be performed for the real-virtual contribution to the single-top production cross section, which refers to the one-loop, non-factorisable corrections to the process in eq. (2.10). By analogy with eq. (3.1), we define

$$\begin{aligned}F^{\rm nf}_{\rm LV}\,(1_q,2_b,3_{q'},4_t;5_g) = &\mathcal{N}\int {\rm dLips}_{34}\,(2\pi)^d\,\delta^{(d)}\left(p_1+p_2-\sum_{i=3}^{5}p_i\right)\\ &\times\; 2{\rm Re}\Big[\mathcal{M}_0^*(1_q,2_b,3_{q'},4_t;5_g)\,\mathcal{M}_1(1_q,2_b,3_{q'},4_t;5_g)\Big]_{\rm nf}\,.\end{aligned} \tag{3.9}$$

We obtain the real-virtual cross section by integrating $F^{\rm nf}_{\rm LV}$ over the phase space of the gluon 5_g. Again, thanks to the fact that the non-factorisable corrections are, effectively, Abelian and no collinear singularities are present, we can extract all singularities related to the emitted gluon by simply subtracting its soft limit. The real-virtual contribution reads

$$\begin{aligned}2s\cdot\sigma_{\rm RV} &= \int [{\rm d}p_5]\,F^{\rm nf}_{\rm LV}\,(1_q,2_b,3_{q'},4_t;5_g)\\ &= \big\langle S_5 F^{\rm nf}_{\rm LV}(1_q,2_b,3_{q'},4_t;5_g)\big\rangle + \big\langle (I-S_5) F^{\rm nf}_{\rm LV}(1_q,2_b,3_{q'},4_t;5_g)\big\rangle\,.\end{aligned} \tag{3.10}$$

The first term is soft-divergent in the radiation phase space, and the corresponding singularities become manifest once the integration over $[{\rm d}p_5]$ is performed. The second term is soft-regulated. We notice that both contributions contain explicit poles in ϵ, stemming from $\mathcal{M}_1$ which appears in the definition of $F^{\rm nf}_{\rm LV}$. We first analyse the soft-divergent term. Using the results in eqs. (2.19) and (3.5) we extract and integrate the soft factor, which multiplies a four-point, one-loop contribution. In order to make all divergences explicit, we exploit eq. (2.4) and obtain

$$\begin{aligned}&\big\langle S_5\,F^{\rm nf}_{\rm LV}\,(1_q,2_b,3_{q'},4_t;5_g)\big\rangle =\\ &\quad-\left(\frac{\alpha_s}{2\pi}\right)^2\frac{N^2-1}{N^2}\left(\frac{2E_{\rm max}}{\mu}\right)^{-2\epsilon}\big\langle K_{\rm nf}(\epsilon)\,{\rm Re}[I_1(\epsilon)]\,F_{\rm LM}(1_q,2_b,3_{q'},4_t)\big\rangle\\ &\quad-\left(\frac{\alpha_s}{2\pi}\right)^2\frac{N^2-1}{2}\left(\frac{2E_{\rm max}}{\mu}\right)^{-2\epsilon}\big\langle K_{\rm nf}(\epsilon)\,\widetilde{F}^{\rm nf}_{\rm LV,fin}(1_q,2_b,3_{q'},4_t)\big\rangle\,,\end{aligned} \tag{3.11}$$

where the last term is proportional to the finite remainder of the single-virtual correction to the elastic process, eq. (2.1). In particular, we have introduced

$$\begin{aligned}\widetilde{F}^{\rm nf}_{\rm LV,fin}(1_q,2_b,3_{q'},4_t) = \mathcal{N}\int {\rm dLips}_{34}\,(2\pi)^d\,\delta^{(d)}(p_1+p_2-p_3-p_4)\\ \times 2{\rm Re}\Big[A_0^*(1_q,2_b,3_{q'},4_t)B_{1,\rm fin}(1_q,2_b,3_{q'},4_t)\Big]\,,\end{aligned} \tag{3.12}$$

which is free of singularities, both explicit and implicit.

We now turn to the soft-regulated term in the second line of eq. (3.10). According to eqs. (2.16) and (2.17), it only contains explicit poles and can be cast into the following form

$$\begin{aligned}&\big\langle (I-S_5)F^{\rm nf}_{\rm LV}(1_q,2_b,3_{q'},4_t;5_g)\big\rangle\\ &\quad=\left(\frac{\alpha_s}{2\pi}\right)\frac{N^2-1}{2}\left\langle {\rm Re}[I_1(\epsilon)]\,(I-S_5)\,\widetilde{F}^{\rm nf}_{\rm LM}(1_q,2_b,3_{q'},4_t;5_g)\right\rangle\\ &\quad+\left(\frac{\alpha_s}{2\pi}\right)\frac{N^2-1}{4}\left\langle (I-S_5)\,\widetilde{F}^{\rm nf}_{\rm LV,fin}(1_q,2_b,3_{q'},4_t;5_g)\right\rangle,\end{aligned} \tag{3.13}$$

with $\widetilde{F}^{\rm nf}_{\rm LM}(1_q,2_b,3_{q'},4_t;5_g)$ given in eq. (3.8). The last contribution in the above equation is related to the finite remainder of the one-loop, five-point amplitude through the definition

$$\begin{aligned}\widetilde{F}^{\rm nf}_{\rm LV,fin}(1_q,2_b,3_{q'},4_t;5_g) = \mathcal{N}\int {\rm dLips}_{34}\,(2\pi)^d\,\delta^{(d)}\left(p_1+p_2-\sum_{i=3}^{5}p_i\right)\\ \times g_{s,b}^2\Big(A_0^{L*}(1_q,2_b,3_{q'},4_t;5_g)B^{sH}_{1,\rm fin}(1_q,2_b,3_{q'},4_t;5_g)\\ +A_0^{H*}(1_q,2_b,3_{q'},4_t;5_g)B^{sL}_{1,\rm fin}(1_q,2_b,3_{q'},4_t;5_g)+{\rm c.c.}\Big)\,.\end{aligned} \tag{3.14}$$

We note that the finite remainders $B^{sL}_{1,\rm fin}$ and $B^{sH}_{1,\rm fin}$ require a dedicated calculation that is discussed in section 4.2.

3.3 Double-virtual cross section

In the previous sections we constructed subtraction terms for the double-real and the real-virtual contributions to the cross section, $\sigma_{\rm RR}$ and $\sigma_{\rm RV}$ respectively. These subtraction terms were integrated over the unresolved phase space resulting in $1/\epsilon$ poles. Moreover, we isolated the divergent part of the real-virtual amplitude and made all the singularities affecting this contribution explicit. These ϵ poles have to cancel against ϵ poles in the double-virtual contributions, which follow from eq. (2.9). The double-virtual cross section can be written as

$$\begin{aligned}2s\cdot\sigma_{\rm VV} &= \big\langle F^{\rm nf}_{\rm LVV}(1_q,2_b,3_{q'},4_t)\big\rangle\\ &=\mathcal{N}\int {\rm dLips}_{34}\,(2\pi)^d\,\delta^{(d)}\Big(p_1+p_2-p_3-p_4\Big)\\ &\quad\times\Big\{|\mathcal{M}_1(1_q,2_b,3_{q'},4_t)|^2_{\rm nf}+2{\rm Re}\Big[\mathcal{M}_0^*(1_q,2_b,3_{q'},4_t)\mathcal{M}_2((1_q,2_b,3_{q'},4_t)\Big]_{\rm nf}\Big\}\\ &=\left(\frac{\alpha_s}{2\pi}\right)^2\frac{N^2-1}{4}\left[\frac{2}{N^2}\Big\langle\big({\rm Re}\,[I_1(\epsilon)]\big)^2F_{\rm LM}(1_q,2_b,3_{q'},4_t)\Big\rangle\right.\\ &\qquad\left.+2\,\big\langle{\rm Re}\,[I_1(\epsilon)]\,\widetilde{F}^{\rm nf}_{\rm LV,fin}(1_q,2_b,3_{q'},4_t)\big\rangle+\big\langle\widetilde{F}^{\rm nf}_{\rm VV,fin}(1_q,2_b,3_{q'},4_t)\big\rangle\right],\end{aligned} \tag{3.15}$$

JHEP06(2022)061

where the first term in the square brackets collects all $1/\epsilon^2$ poles, the second contribution only contains $1/\epsilon$ poles, while the last term is finite. We note that $\widetilde{F}^{\rm nf}_{\rm LV,fin}$ is defined in eq. (3.12) and that $\widetilde{F}^{\rm nf}_{\rm VV,fin}$ reads

$$\begin{aligned}\widetilde{F}^{\rm nf}_{\rm VV,fin}(1_q,2_b,3_{q'},4_t) = \mathcal{N}\int {\rm dLips}_{34}\,(2\pi)^d\,\delta^{(d)}(p_1+p_2-p_3-p_4)\\ \times\left\{\left|B_{1,\rm fin}(1_q,2_b,3_{q'},4_t)\right|^2+2{\rm Re}\Big[A_0^*(1_q,2_b,3_{q'},4_t)B_{2,\rm fin}(1_q,2_b,3_{q'},4_t)\Big]\right\}.\end{aligned} \tag{3.16}$$

3.4 Pole cancellation

To obtain a manifestly finite expression for the non-factorisable contribution to the total cross section we need to sum the results in eqs. (3.6), (3.11), (3.13) and (3.15). It is convenient to write this sum as the combination of three different terms corresponding to final states with different resolved multiplicities. We write

$$\sigma_{\rm nf} = \sigma_{\rm nf}^{(2g)} + \sigma_{\rm nf}^{(1g)} + \sigma_{\rm nf}^{(0g)}, \tag{3.17}$$

where

$$2s\cdot\sigma_{\rm nf}^{(2g)} = \left\langle (I-S_5)(I-S_6)F^{\rm nf}_{\rm LM}\left(1_q,2_b,3_{q'},4_t;5_g,6_g\right)\right\rangle \tag{3.18}$$

is the fully regulated double-real emission contribution. It can be directly implemented in a numerical program. In order to present the single-real emission contribution, $\sigma_{\rm nf}^{(1g)}$, and the elastic contribution, $\sigma_{\rm nf}^{(0g)}$, we introduce the following function

$$\mathcal{W}(1_q,2_b,3_{q'},4_t) = \left(\frac{2E_{\rm max}}{\mu}\right)^{-2\epsilon} K_{\rm nf}(1_q,2_b,3_{q'},4_t;\epsilon) - {\rm Re}[I_1(1_q,2_b,3_{q'},4_t;\epsilon)]\,. \tag{3.19}$$

We point out that $\mathcal{W}$ does not contain any ϵ pole. In fact, the first term in the ϵ-expansion of $K_{\rm nf}$ describes a soft, wide-angle emission and assumes a simple form

$$K_{\rm nf}(1_q,2_b,3_{q'},4_t;\epsilon) = \frac{1}{\epsilon}\,\log\left(\frac{p_1\cdot p_4\; p_2\cdot p_3}{p_1\cdot p_2\; p_3\cdot p_4}\right)+\mathcal{O}(\epsilon^0)\,. \tag{3.20}$$

Such a pole is cancelled by the singularities arising from single-virtual corrections. In particular, using eq. (2.5), we find

$$K_{\rm nf}(1_q,2_b,3_{q'},4_t;\epsilon) - {\rm Re}\big[I_1(1_q,2_b,3_{q'},4_t;\epsilon)\big] = \mathcal{O}(\epsilon^0)\,. \tag{3.21}$$

The single-real emission contribution, which corresponds to the sum of eq. (3.13) and the second term in eq. (3.6), is then equal to

$$\begin{aligned}2s\cdot\sigma_{\rm nf}^{(1g)} = &-\left(\frac{\alpha_s}{2\pi}\right)\frac{N^2-1}{2}\left\langle\mathcal{W}(1_q,2_b,3_{q'},4_t)(I-S_5)\widetilde{F}^{\rm nf}_{\rm LM}(1_q,2_b,3_{q'},4_t;5_g)\right\rangle\\ &+\left(\frac{\alpha_s}{2\pi}\right)\frac{N^2-1}{4}\left\langle(I-S_5)\widetilde{F}^{\rm nf}_{\rm LV,fin}(1_q,2_b,3_{q'},4_t;5_g)\right\rangle.\end{aligned} \tag{3.22}$$

JHEP06(2022)061

It is free of both explicit and implicit singularities. Finally, the finite, elastic contribution becomes

$$\begin{aligned} 2s \cdot \sigma_{\text{nf}}^{(0g)} = &\left(\frac{\alpha_s}{2\pi}\right)^2 \frac{N^2-1}{2N^2} \left\langle \mathcal{W}^2(1_q, 2_b, 3_{q'}, 4_t)\, F_{\text{LM}}(1_q, 2_b, 3_{q'}, 4_t) \right\rangle \\ &- \left(\frac{\alpha_s}{2\pi}\right)^2 \frac{N^2-1}{2} \left\langle \mathcal{W}(1_q, 2_b, 3_{q'}, 4_t)\, \widetilde{F}^{\text{nf}}_{\text{LV,fin}}(1_q, 2_b, 3_{q'}, 4_t) \right\rangle \\ &+ \left(\frac{\alpha_s}{2\pi}\right)^2 \frac{N^2-1}{4} \left\langle \widetilde{F}^{\text{nf}}_{\text{VV,fin}}(1_q, 2_b, 3_{q'}, 4_t) \right\rangle . \end{aligned} \tag{3.23}$$

As a final remark in this section, it is worth noting that in the entire procedure described here, the only amplitude which must be expanded to $\mathcal{O}(\epsilon)$ is $B_1(1_q, 2_b, 3_{q'}, 4_t)$ as it is needed to extract the two-loop finite remainder $B_{2,\text{fin}}(1_q, 2_b, 3_{q'}, 4_t)$ in eq. (2.7).

4 Amplitude calculation

In this section we discuss the calculation of the amplitudes needed to compute the non-factorisable cross-section defined in eq. (3.17). The obtention of the three tree-level amplitudes is shortly described, followed by the one- and two-loop amplitudes.

4.1 Tree-level amplitudes

To compute real-emission amplitudes we generate the relevant diagrams with `QGRAF` [42] and process them in `FORM` [43, 44]. As single-top production is facilitated by the exchange of a W boson, all massless quarks that appear in these amplitudes are left-handed. This can be seen at the diagram level by using the anti-commutativity of γ_5 to move the spin projectors $P_L = \frac{1}{2}(1-\gamma_5)$ from the W vertices to the incoming massless fermions. Using standard bracket notation from spinor helicity formalism,[4] we write

$$P_L\, u(p_i) = u_L(p_i) = |i]\,, \quad \text{for light-like } p_i. \tag{4.1}$$

This fixes the helicity of the three massless external fermions, while the outgoing massive top quark can be both left- and right-handed. By decomposing the momentum of the top quark into two massless momenta

$$p_4 = p_4^\flat + \frac{m_t^2}{2n \cdot p_4}\, n\,, \tag{4.2}$$

the massive Dirac-conjugate spinor can be written as

$$\bar{u}_L(p_4) = \langle 4^\flat| + \frac{m_t}{[n4^\flat]}[n| \quad \text{and} \quad \bar{u}_R(p_4) = [4^\flat| + \frac{m_t}{\langle n4^\flat\rangle}\langle n|\,. \tag{4.3}$$

With these definitions we can write tree-level helicity amplitudes as

$$\begin{aligned} A_0(1_q^L, 2_b^L, 3_{q'}^L, 4_t^L) &= \frac{g_W^2}{t-m_W^2}\langle 34^\flat\rangle[21]\,, \\ A_0(1_q^L, 2_b^L, 3_{q'}^L, 4_t^R) &= \frac{g_W^2}{t-m_W^2}\frac{m_t}{\langle n4^\flat\rangle}\langle 3n\rangle[21]\,, \end{aligned} \tag{4.4}$$

[4] For a review of spinor-helicity formalism, see e.g. ref. [45]. For the case of massive fermions, see also ref. [46].

JHEP06(2022)061

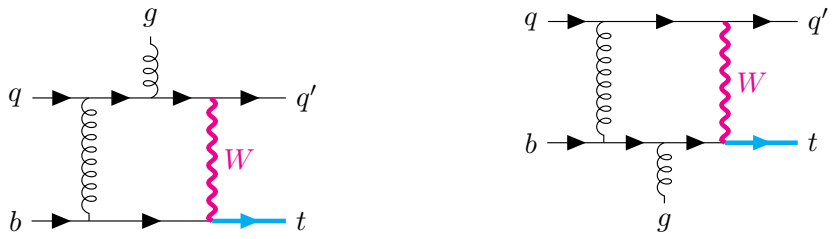

Figure 2. Examples of diagrams contributing to amplitudes $B_1^{sL}(5_g)$ (left) and $B_1^{sH}(5_g)$ (right) as defined through colour decomposition in eq. (2.15).

where $t = (p_1 - p_3)^2$ and $g_W = 2m_W/v$ is the weak coupling constant defined through the W boson mass, m_W, and the Higgs field vacuum expectation value, v. By choosing $n = p_3$, we can force the latter amplitude to vanish; this, in turn yields more compact results for higher-multiplicity amplitudes. The tree-level amplitudes have been cross-checked against `MadGraph5_aMC@NLO` [47].

4.2 Loop amplitudes

We computed the non-factorisable four-point, one-loop amplitude $B_1(1_q, 2_b, 3_{q'}, 4_t)$ defined in eq. (2.3), in an earlier paper [39]. This amplitude enters the present calculation in both the real-virtual and double-virtual cross sections, see eqs. (3.10) and (3.15) respectively. We note that $\mathcal{O}(\epsilon)$ terms are only required for the latter for which we use the results obtained numerically for a fixed grid of phase space points in ref. [39]. For the real-virtual contribution, amplitudes through $\mathcal{O}(\epsilon^0)$ are needed. To evaluate them, we rely on `QCDLoops` [48, 49] for efficient and precise computation of one-loop integrals.

The real-virtual contribution to the cross section also depends on the one-loop, five-point amplitude $\mathcal{M}_1(1_q, 2_b, 3_{q'}, 4_t; 5_g)$ defined in eq. (2.15). The relevant colour-stripped amplitudes involve a gluon exchange between the fermion lines as well as a gluon emission. The non-factorisable contribution to the cross section comes from interference between diagrams where the final-state gluon is emitted and absorbed by different fermion lines. Diagrams with a non-Abelian gluon vertex do not contribute to the cross section due to colour conservation, cf. eq. (2.16). For a straightforward extraction of the non-factorisable contribution, we calculate amplitudes for gluon emission from each of the two quark lines separately, B_1^{sL} and B_1^{sH}. In figure 2 we present example diagrams for these two amplitudes.

A total of 24 diagrams contribute to B_1^{sL} and B_1^{sH}. We generate them with `QGRAF` and process using `FORM`. We restrict external momenta to four dimensions, while loop momenta are considered to be d-dimensional. Hence, the amplitude contains chains of Dirac matrices with d-dimensional indices between four-dimensional spinors. The extra-dimensional part can be extracted by decomposing the matrices in four- and (-2ϵ)-dimensional parts, $\gamma^\mu = \gamma^{\bar{\mu}} + \gamma^{\tilde{\mu}}$. Indices with bars are restricted to four dimensions and indices with tilde are (-2ϵ)-dimensional. Spinor chains involving indices living in extra-dimensional space are projected on to tensors consisting solely of metric tensors restricted to the (-2ϵ)-dimensional

JHEP06(2022)061

subspace. As an example, we write

$$\overline{u}_t(p_4)\gamma^\mu\gamma^\nu u_b(p_2) = \overline{u}_t(p_4)\gamma^{\bar{\mu}}\gamma^{\bar{\nu}} u_b(p_2) + g^{\tilde{\mu}\tilde{\nu}}\,\overline{u}_t(p_4)u_b(p_2)\,. \tag{4.5}$$

After this procedure is applied, all spinor chains involve objects with four-dimensional indices so that helicity amplitudes can be computed straightforwardly. As we already mentioned, due to the W boson vertex all massless fermions are left-handed, hence there is a total of four helicity configurations. The step of dimension splitting and helicity configuration projection is handled by the `FORM` library `spinney` [50].

At this stage B_1^{sL} and B_1^{sH} can be written as linear combinations of Feynman integrals, I, weighted by coefficients c. We write

$$B_1^{sX} = \sum_i \sum_{r=0}^{3} c^X_{5,i,r}(\epsilon)\, I_{5,i}[k^{\mu_1}\cdots k^{\mu_r}] + \sum_i \sum_{r=0}^{2} c^X_{4,i,r}(\epsilon)\, I_{4,i}[k^{\mu_1}\cdots k^{\mu_r}]\,, \tag{4.6}$$

where $X = L, H$ and index i labels the integral topology. The coefficients acquire dependence on space-time dimension because of the dimension-splitting procedure described above. For brevity, we have suppressed their dependence on kinematic invariants, four-dimensional spinor structures, and the electroweak coupling. The integrals $I_{n,i}$ include pentagons ($n = 5$) of up to rank 3 and boxes ($n = 4$) of up to rank 2. We write

$$I_{n,i}[k^{\mu_1}\cdots k^{\mu_r}] = \int \frac{\mathrm{d}^d k}{(2\pi)^d} \frac{\prod_{j=1}^{r} k^{\mu_j}}{\prod_{l=1}^{n} D_{i,l}}\,, \tag{4.7}$$

where $D_{i,l} = (k - q_{i,l})^2 - m^2_{i,l}$ and the $q_{i,l}$ are given by sums of external momenta. The propagator masses $m_{i,k}$ are zero, m_t, or m_W.

The most complicated integrals in eq. (4.6) are tensor pentagon integrals of rank 3. We reduce them to boxes of rank 2 and scalar pentagons by expanding the integrand numerator using the van Neerven-Vermaseren (vNV) basis [51]. We note that up to rank 3, pentagon integrals are free of rational terms [52] and the expansion of the loop momentum in four dimensions is sufficient to obtain correct results in the $d \to 4$ limit. Hence, we expand the loop momentum as

$$k^\mu = \sum_{i=1}^{4} (k \cdot q_i)\, v_i^\mu\,, \tag{4.8}$$

where we have used the fact that scalar products of vNV basis vectors v_i and propagator momenta q_j satisfy $v_i \cdot q_j = \delta_{ij}$. The scalar products $(k \cdot q_i)$ can be written in terms of kinematic invariants and inverse propagators. We also note that $v_i^2 \neq 0$. Applying this procedure, we obtain

$$\begin{aligned} B_1^{sX} = &\sum_i \tilde{c}^X_{5,i,0}(\epsilon)\, I_{5,i} + \sum_i \sum_{r=0}^{2} \tilde{c}^X_{4,i,r}(\epsilon)\, I_{4,i}[k^{\mu_1}\cdots k^{\mu_r}] \\ &+ \sum_i \sum_{r=0}^{1} \tilde{c}^X_{3,i,r}(\epsilon)\, I_{3,i}[k^{\mu_1}\cdots k^{\mu_r}] + \sum_i \tilde{c}^X_{2,i,0}(\epsilon)\, I_{2,i}\,, \end{aligned} \tag{4.9}$$

JHEP06(2022)061

where we introduced the shorthand notation $I_{n,i}[1] \equiv I_{n,i}$. At this stage we are left with scalar pentagon integrals and tensor integrals with at most four propagators. Up to finite order in ϵ, scalar pentagon integrals can be rewritten as boxes [53]. The rest of the calculation employs the Passarino-Veltman reduction [54] that allows us to express the amplitude through scalar integrals. We obtain

$$B_1^{sX} = \sum_i \hat{c}_{4,i}^X(\epsilon)\, I_{4,i} + \sum_i \hat{c}_{3,i}^X(\epsilon)\, I_{3,i} + \sum_i \hat{c}_{2,i}^X(\epsilon)\, I_{2,i} + \mathcal{O}(\epsilon)\,. \tag{4.10}$$

After reduction the amplitude can be written in terms of 109 scalar box, triangle, and bubble integrals. By switching to a basis with finite box integrals, the complexity of the integral coefficients reduces drastically. We construct this basis following the ideas presented in ref. [55]. As an example of this basis change, we consider one of the box integrals

$$I_{4,1} = \int \frac{\mathrm{d}^d k}{(2\pi)^d} \frac{1}{k^2 (k-p_1)^2 (k-p_1-p_2)^2 (k-p_1-p_2+p_5)^2}\,, \tag{4.11}$$

that is infrared-divergent and the leading divergence is the second-degree ϵ pole. These singularities develop when one of the propagators goes on shell, for example when $k \to 0$ or $k \to p_1$.

We can regulate these singularities by introducing an appropriate numerator in the integrand. A suitable numerator insertion vanishes in the limits where the propagators that develop singularities go on shell. For the integral in eq. (4.11) we use the following insertion

$$\begin{aligned} \mathrm{tr}\left((-\not{p}_1)(\not{k}-\not{p}_1)(\not{k}-\not{p}_1-\not{p}_2)(\not{p}_5)\right) &= -s_{12}\,(s_{12}+s_{15}-s_{34}) + (s_{12}+s_{15}-s_{34})\,k^2 \\ &- (s_{12}-s_{34})\,(k-p_1)^2 + (s_{12}+s_{15})\,(k-p_1-p_2)^2 - s_{12}\,(k-p_1-p_2+p_5)^2\,. \end{aligned} \tag{4.12}$$

We introduced $\not{p} = \gamma^\mu p_\mu$, as well as the usual Mandelstam variables $s_{ij} = (p_i + \lambda_{ij} p_j)^2$ with $\lambda_{ij} = 1$ if the partons i and j are both incoming or outgoing and $\lambda_{ij} = -1$ otherwise. With this, we define the finite box integral

$$F_{4,1} = \int \frac{\mathrm{d}^d k}{(2\pi)^d} \frac{\mathrm{tr}\left((-\not{p}_1)(\not{k}-\not{p}_1)(\not{k}-\not{p}_1-\not{p}_2)(\not{p}_5)\right)}{k^2 (k-p_1)^2 (k-p_1-p_2)^2 (k-p_1-p_2+p_5)^2} = \mathcal{O}(\epsilon^0)\,. \tag{4.13}$$

It is clear from eq. (4.12) that the finite box is a linear combination of the divergent box and four triangle integrals. Replacing all divergent boxes in the integral basis with their finite counter-parts therefore changes the triangle coefficients while leaving the box coefficients unchanged (up to an overall kinematic factor). Hence, we obtain

$$B_1^{sX} = \sum_i \bar{c}_{4,i}^X\, F_{4,i} + \sum_i \bar{c}_{3,i}^X\, I_{3,i} + \sum_i \hat{c}_{2,i}^X(\epsilon)\, I_{2,i} + \mathcal{O}(\epsilon)\,. \tag{4.14}$$

We note that the most complicated coefficients in the amplitude appear in front of the finite box integrals. However, since these integrals are finite we can set $\epsilon \to 0$ in their coefficients. Furthermore, since in this basis ϵ^{-2} poles only appear in triangle integrals, their coefficients must be simple. In fact, after the procedure described above is applied, the triangle integral coefficients either become independent of space-time dimension or simply

JHEP06(2022)061

vanish. We note that due to the fact that the amplitude that we compute is UV-finite, the sum of bubble integrals is finite as well.

One of the challenges in computing the real-virtual contribution to the cross section is that we need to compute the amplitude in the limit when the emitted gluon is soft. To improve numerical stability in the evaluation of the amplitudes, we write the integral coefficients in terms of the kinematic invariants

$$s_{12}, \quad s_{23}, \quad \delta_1 = s_{34} - s_{12}, \quad \delta_2 = s_{45} - m_t^2, \quad \delta_3 = s_{15}\,. \tag{4.15}$$

In the limit where the emitted gluon goes soft, $p_5 \to 0$, the δ-variables vanish. Because of that, large cancellations in the integral coefficients can be avoided.

We have checked the real-virtual amplitude in several ways. First, we compared its ϵ poles with expectations shown in eq. (2.17). We have also checked the factorisation in the limit where the emitted gluon goes soft, cf. eq. (2.19).

As a final remark, we note that the two-loop amplitude which is needed for the double-virtual contribution was computed in a previous paper [39]. We used those results for the $q\,b \to q'\,t$ channel and obtained the contribution of the $\overline{q}\,b \to \overline{q}'\,t$ channel through the crossing symmetry, $p_1 \leftrightarrow -p_3$. We note that no additional master integrals are required since after crossing the amplitude can be mapped back to the basis of master integrals using integration-by-parts identities.

5 Results

In this section we discuss the phenomenology of the non-factorisable corrections to single-top production at the LHC. Our starting point is the conventional formula for the differential cross section

$$\mathrm{d}\sigma_{pp\to X+t} = \sum_{i,j} \int \mathrm{d}x_1\,\mathrm{d}x_2\; f_i(x_1,\mu_F)\, f_j(x_2,\mu_F)\; \mathrm{d}\hat{\sigma}_{ij\to X+t}\,(x_1,x_2)\;, \tag{5.1}$$

where we sum over partons that participate in the hard scattering.

We take the CKM matrix to be an identity matrix and work in the five-flavour scheme. The top quark in the final state is produced in the collisions of a bottom quark from a proton and a virtual W boson. Overall, the cross section in eq. (5.1) receives contributions from processes with $i(j) = b$ and $j(i) = u, c, \bar{d}, \bar{s}$.

We consider proton-proton collisions at 13 TeV and use the PDF set `CT14` in the computation. We obtain the leading-order cross sections and distributions using the leading-order PDFs `CT14_lo` and the NNLO non-factorisable contribution using the `CT14_nnlo` PDF set. The strong coupling constant is provided by the `CT14_nnlo` PDF set; numerically it evaluates to $\alpha_s(m_Z) = 0.118$. As the input parameters, we use the vacuum expectation value of the Higgs field, $v = 246.2$ GeV, the mass of the W boson, $m_W = 80.379\,\mathrm{GeV}$, and the pole mass of the top quark, $m_t = 173.0\,\mathrm{GeV}$.

The non-factorisable NNLO QCD correction to the single-top production cross section is found to be

$$\frac{\sigma_{pp\to X+t}}{1\text{ pb}} = 117.96 + 0.26\left(\frac{\alpha_s(\mu_R)}{0.108}\right)^2\,, \tag{5.2}$$

JHEP06(2022)061

where the first term on the right-hand side is the LO cross section and the second is the NNLO non-factorisable correction.[5] To compute the cross sections shown in eq. (5.2), we have set the factorisation scale to $\mu_F = m_t$.

We note however, that since the non-factorisable contributions are absent at NLO due to colour conservation, we do not have any indication of an optimal scale choice. To emphasise this point, we have left the dependence on the renormalisation scale explicit in eq. (5.2). We note that the value of the strong coupling constant used there, $\alpha_s = 0.108$, corresponds to $\mu_R = m_t$ and for this choice of the scale the non-factorisable correction is about 0.2% of the LO cross section.

However, it is unclear whether $\mu_{R,F} = m_t$ is the right choice for the scales. Indeed, a typical momentum transfer in t-channel single-top production is ~ 40 GeV since this is the value for which the top-quark transverse momentum distribution is maximal. If we choose $\mu_R = 40\,\text{GeV}$, the non-factorisable corrections to the leading-order cross section become 0.35%. We note that this result is in line with the recently published finite part of the virtual contribution [39], which was found to be around 0.5% for the same scale choice.

In what follows, we take $\mu_F = \mu_R \equiv \mu$, choose $\mu = m_t$ as the central scale and estimate the scale uncertainty by increasing and decreasing μ by a factor of 2. As we already mentioned, even if we do not consider this choice to be optimal, it does facilitate a comparison with the literature, as it was used in several studies of *factorisable* corrections to single-top production [30, 33]. In addition for a more realistic assessment of the magnitude of non-factorisable corrections, we also show their impact for $\mu = 40\,\text{GeV}$.

We first present results for the top-quark transverse momentum distribution, see figure 3. It follows that non-factorisable corrections are $p_\perp^t$-dependent; they are relatively small and negative at low values of the transverse momentum, vanish at $p_\perp^t \sim \mathcal{O}(50\text{ GeV})$ and reach $\mathcal{O}(2\%)$ at $p_\perp^t \sim 200\,\text{GeV}$. This behaviour is compatible with the fact that virtual contributions are negative in the same $p_\perp^t$ interval [39] and, as we explained in the introduction, virtual contributions to non-factorisable corrections are expected to be dominant. We note that shapes of factorisable and non-factorisable corrections to the $p_\perp^t$ distribution are similar but, typically, the factorisable ones are larger by a factor between 3 and 10, (see figure 11 in ref. [33]). However, it follows from the same figure, that the factorisable corrections vanish around $p_\perp^t \sim 30\,\text{GeV}$ whereas the non-factorisable ones vanish around $p_\perp^t \sim 50\,\text{GeV}$. Hence, the non-factorisable corrections are, in fact, comparable to the factorisable ones in the region around the *maximum* of the $p_\perp^t$ distribution.

In table 1 we report the LO cross sections and the corresponding NNLO corrections for different cuts on the minimal top-quark transverse momentum. We fixed the factorisation scale to $\mu_F = m_t$ and inspect different renormalisation scales. For $\mu_R = m_t$, we notice that, while the LO cross section *decreases* by $\mathcal{O}(11\%)$ if the $p_\perp^t$ cut increases from 0 to 60 GeV, the non-factorisable contribution to the cross section *increases* by $\mathcal{O}(8\%)$. To understand the relative importance of factorisable and non-factorisable NNLO corrections, we note that factorisable corrections were computed to be about -0.7% of the NLO cross section

[5] We stress one more time that the LO cross section in eq. (5.2) is computed with the LO PDFs and the NNLO correction is computed with the NNLO PDFs.

JHEP06(2022)061

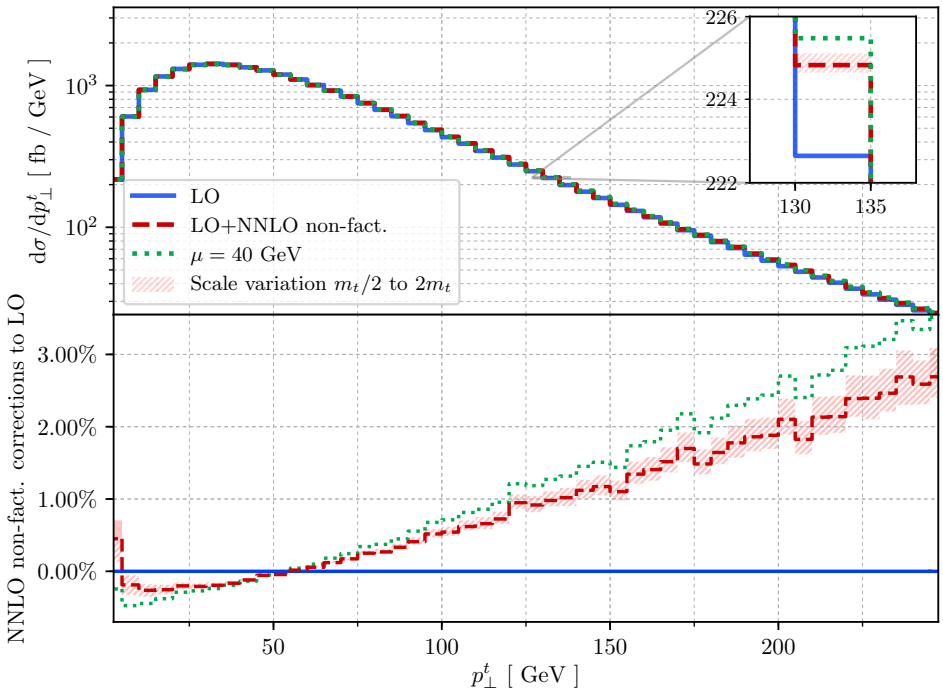

Figure 3. Distribution of the top-quark transverse momentum. The LO distribution is marked with a blue, solid line, while the red, dashed line corresponds to our predictions for the LO+NNLO distribution at $\mu = m_t$. The scale is variated between $\mu = m_t/2$ and $\mu = 2m_t$. The green, dotted line corresponds to the scale $\mu = 40\,\text{GeV}$. The lower pane shows the ratio of non-factorisable corrections to the LO distribution. See text for further details.

		$\mu_R = m_t$		$\mu_R = 40$ GeV	
$p_\perp^{t,\text{cut}}$	σ_{LO} (pb)	$\sigma_{\text{NNLO}}^{\text{nf}}$ (pb)	δ_{NNLO} [%]	$\sigma_{\text{NNLO}}^{\text{nf}}$ (pb)	δ_{NNLO} [%]
0 GeV	118.01	$0.26^{-0.04}_{+0.06}$	$0.22^{-0.04}_{+0.05}$	0.40	0.34
20 GeV	115.09	$0.26^{-0.04}_{+0.06}$	$0.23^{-0.04}_{+0.05}$	0.41	0.36
40 GeV	109.56	$0.27^{-0.05}_{+0.06}$	$0.25^{-0.04}_{+0.06}$	0.43	0.39
60 GeV	104.63	$0.28^{-0.05}_{+0.06}$	$0.26^{-0.04}_{+0.06}$	0.43	0.41

Table 1. Dependence of the non-factorisable corrections on the top-quark transverse momentum. The factorisation scale is fixed to $\mu_F = m_t$. In the third column, the non-factorisable cross sections are evaluated at $\mu_R = m_t$ with sub- and super-scripts indicating the scale variation, $m_t/2$ and $2m_t$ respectively. The penultimate column describes the non-factorisable corrections at $\mu_R = 40\,\text{GeV}$. For each scale choice, we report the relative impact, δ_{NNLO}, of the non-factorisable contributions with respect to the LO cross section.

JHEP06(2022)061

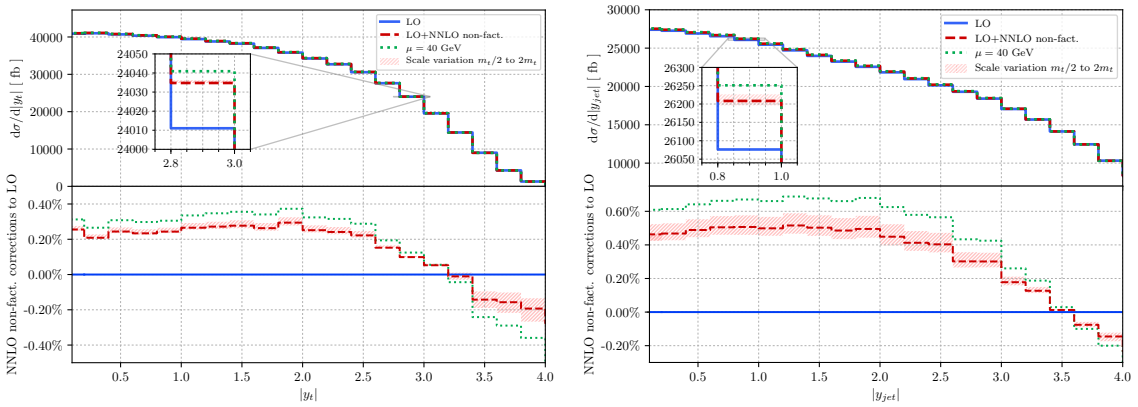

(a) Distribution of the top-quark rapidity.

(b) Distribution of the leading-jet rapidity.

Figure 4. Distributions of the absolute value of the top-quark rapidity (left) and of the leading-jet rapidity (right). LO distributions are marked with a blue, solid line, while red, dashed lines correspond to our predictions for LO+NNLO distributions at $\mu = m_t$. The scale is variated between $\mu = m_t/2$ and $\mu = 2m_t$. The green, dotted line corresponds to the scale $\mu = 40\,\mathrm{GeV}$. Lower panes show the ratio of non-factorisable corrections to LO distributions. See text for further details.

for similar choices of scales and parton distribution functions (see table 7 in ref. [33]).[6] If we compare this result with the fourth column of table 1 we conclude that the impact of non-factorisable corrections is smaller than, but quite comparable to, the factorisable corrections. At $\mu_R = 40\,\mathrm{GeV}$, the NNLO non-factorisable corrections increase by $\mathcal{O}(8\%)$ by imposing a lower cut of 60 GeV on the transverse momentum of the top quark.

The top-quark rapidity distribution is shown in the left pane of figure 4. The (relative) non-factorisable corrections are fairly flat in the interval $|y_t| < 2.5$ and change the leading-order rapidity distribution by $\mathcal{O}(0.25\%)$. For larger rapidity values, the corrections decrease rapidly and change sign at $|y_t| \sim 3$. It follows from ref. [33] that the factorisable corrections to the top-quark rapidity distribution change the sign earlier, at around $|y_t| = 1.2$. Again, for such rapidity values, the non-factorisable and factorisable corrections are quite comparable.

We turn to the analysis of the impact of non-factorisable corrections on jet observables in single-top production. We use the k_t-algorithm [56] to define jets. Jets are required to have transverse momenta larger than 30 GeV and a radius $R = 0.4$.

In figure 4(b) we show the impact of non-factorisable corrections on the leading-jet rapidity distribution. The correction is about 0.5% at small rapidities, $|y_{\mathrm{jet}}| < 2$. Similar to the case of the top-quark rapidity distribution, the correction to leading-jet rapidity decreases and changes sign at around $|y_{\mathrm{jet}}| \sim 3.5$.

In figure 5 we show the transverse momentum distribution of the leading jet (left pane) and the distribution of the sum of the top and jets' transverse momenta,

$$H_\perp = p_\perp^t + \sum_{i=1}^{n_{\mathrm{jet}}} p_\perp^{\mathrm{jet},i}\,. \tag{5.3}$$

[6] Computations in ref. [33] were performed for proton-proton collisions at 14 TeV.

JHEP06(2022)061

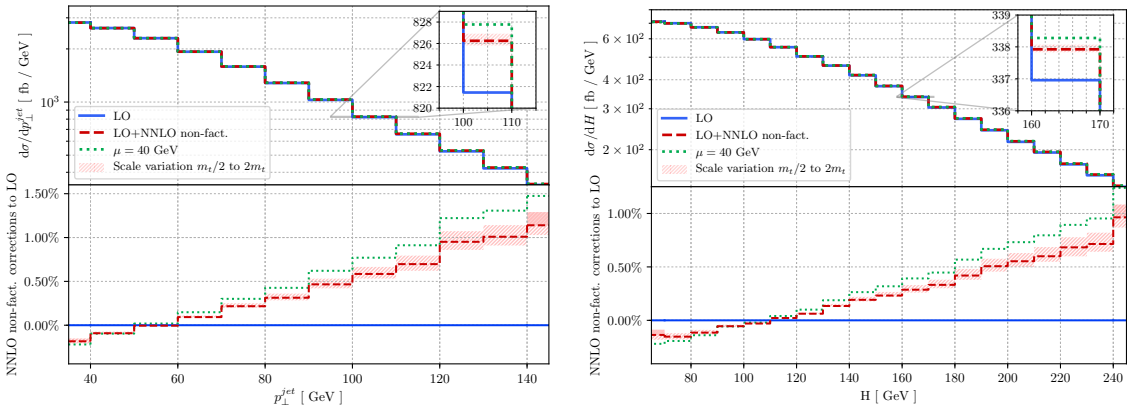

(a) Distribution of the leading-jet transverse momentum.

(b) Distribution of the sum of transverse momenta H.

Figure 5. Distributions of the leading-jet transverse momentum (left) and of sum of transverse momenta H defined in eq. (5.3) (right). LO distributions are marked with a blue, solid line, while red, dashed lines correspond to our predictions for LO+NNLO distributions at $\mu = m_t$. The scale is variated between $\mu = m_t/2$ and $\mu = 2m_t$. The green, dotted line corresponds to the scale $\mu = 40\,\text{GeV}$. Lower panes show the ratio of non-factorisable corrections to LO distributions. See text for further details.

In eq. (5.3) n_{jet} is the number of reconstructed jets in an event. The corrections to the leading-jet transverse momentum distributions change sign around 50 GeV, are negative for smaller $p_\perp^{\text{jet}}$ values and grow to about 1.2 percent at $p_\perp^{\text{jet}} \sim 140$ GeV. The distribution of the sum of transverse momenta H is affected by the non-factorisable corrections in a similar way.

6 Conclusions

In this paper we have computed the non-factorisable corrections to t-channel single-top production at the LHC. This contribution, being colour-suppressed and computationally challenging, was neglected in all the previous studies of NNLO QCD corrections to single-top production in spite of the recent indication that a peculiar enhancement of such corrections due to remnants of the Glauber phase is possible [36].

We have shown how to overcome the technical challenges related to the computation of virtual, non-factorisable corrections in ref. [39]. In this paper we completed the calculation of these corrections by including double-real and real-virtual contributions required to obtain the infrared-finite cross section. We have discussed the calculation of the relevant tree- and one-loop amplitudes needed for the computation of non-factorisable corrections. Because of the large number of mass scales that appear in the computation of one-loop amplitudes required for the real-virtual non-factorisable contribution, its reduction to master integrals, and its stable and efficient numerical evaluation turn out to be non-trivial. We discussed how to address these problems and pointed out that it is beneficial to choose infrared-finite combinations of boxes and triangles as master integrals.

JHEP06(2022)061

We have explicitly shown that the non-factorisable corrections are not affected by the non-Abelian nature of QCD and are free of collinear singularities. We have constructed subtraction terms that make the cancellation of infra-red singularities in arbitrary infrared-safe observables explicit.

We have studied a number of kinematic distributions relevant for the single-top production process as well as the inclusive cross section. We have found that non-factorisable corrections are smaller than, but quite comparable to, the factorisable ones. Since the choice of the proper renormalisation scale in the non-factorisable corrections is an open issue, the actual magnitude of these corrections is uncertain. We estimate that they can reach $\mathcal{O}(0.4\%)$ in case of the inclusive cross section and $\mathcal{O}(1-2\%)$ for some kinematic distributions. Another interesting point is that for many distributions the non-factorisable corrections *do not* reduce to an overall renormalisation of the leading-order distributions. Thus, if a percent-level precision in single-top studies can be reached, the non-factorisable effects will have to be taken into account.

Acknowledgments

C. S-S. would like to thank Paolo Torrielli for useful discussions. This research is partially supported by the Deutsche Forschungsgemeinschaft (DFG, German Research Foundation) under grant 396021762 — TTR 257. The diagrams in figure 1 and 2 were generated using `tikz-feynman` [57].

A Renormalisation

Since the non-factorisable NLO QCD corrections vanish due to colour conservation, there is no UV divergences at NNLO. Nevertheless, the coupling is renormalised in $\overline{\text{MS}}$ scheme to zeroth order in perturbative QCD

$$\frac{g_{s,b}^2}{4\pi} \equiv \alpha_s^{\text{bare}} = \mu^{2\epsilon} S_\epsilon \, \alpha_s(\mu) \,, \tag{A.1}$$

where $S_\epsilon = \exp(\epsilon\gamma_E)/(4\pi)^\epsilon$ and $\gamma_E \approx 0.57721$ is the Euler-Mascheroni constant.

B Integrated counterterms

In this section we describe the calculation of the single-soft integrated counterterms. As explained in the main body of the paper, it is important for treating the infrared singularities that originate from the real radiation. We have previously defined the function $K_{\text{nf}}(\epsilon)$ through the following integral

$$g_{s,b}^2 \int [\mathrm{d}p_k] \, \text{Eik}_{\text{nf}}(1_q, 2_b, 3_{q'}, 4_t; k_g) = \frac{\alpha_s}{2\pi} \left(\frac{2E_{\text{max}}}{\mu}\right)^{-2\epsilon} K_{\text{nf}}(1_q, 2_b, 3_{q'}, 4_t; \epsilon) \,. \tag{B.1}$$

Again, we stress that the coupling $g_{s,b}$ appearing on the left-hand side of eq. (B.1) is the bare coupling constant, while on the right-hand side α_s is the coupling renormalised at

JHEP06(2022)061

the scale μ. The latter is obtained by using the prescription in appendix A. Moreover, we have defined

$$\begin{aligned}\mathrm{Eik}_{\mathrm{nf}}(1_q,2_b,3_{q'},4_t;k_g) &= \sum_{\substack{i\in[1,3]\\ j\in[2,4]}} \frac{\lambda_{ij}\, p_i\cdot p_j}{(p_i\cdot p_k)\,(p_j\cdot p_k)} \\ &= \frac{p_1\cdot p_2}{p_1\cdot p_k\, p_2\cdot p_k} - \frac{p_1\cdot p_4}{p_1\cdot p_k\, p_4\cdot p_k} - \frac{p_2\cdot p_3}{p_2\cdot p_k\, p_3\cdot p_k} + \frac{p_3\cdot p_4}{p_3\cdot p_k\, p_4\cdot p_k}\,.\end{aligned} \tag{B.2}$$

We note that the above expression involves two different structures: eikonal factors that depend on the four-momenta of two massless partons, and eikonal factors that depend on the four-momenta of one massive and one massless parton. The integration over the unresolved radiation is different in the two cases.

Before proceeding with the details of the calculation, we quote the final result in order to highlight its simplicity. The result reads

$$\begin{aligned}K_{\mathrm{nf}}(1_q,2_b,3_{q'},4_t;\epsilon) = \frac{1}{\epsilon}\,\log\left(\frac{p_1\cdot p_4\; p_2\cdot p_3}{p_1\cdot p_2\; p_3\cdot p_4}\right) &- \frac{1}{2}\log^2\left(\frac{\rho_{23}}{2}\right) + \frac{1}{2}\log^2\left(\frac{\rho_{12}}{2}\right) \\ &- \log\left(\frac{\rho_{14}}{1-\beta}\right)\log\left(\frac{\rho_{14}}{1+\beta}\right) + \log\left(\frac{\rho_{34}}{1-\beta}\right)\log\left(\frac{\rho_{34}}{1+\beta}\right) \\ &+ \mathrm{Li}_2\left(1-\frac{\rho_{12}}{2}\right) - \mathrm{Li}_2\left(1-\frac{\rho_{23}}{2}\right) \\ &- \mathrm{Li}_2\left(1-\frac{\rho_{14}}{1-\beta}\right) - \mathrm{Li}_2\left(1-\frac{\rho_{14}}{1+\beta}\right) \\ &+ \mathrm{Li}_2\left(1-\frac{\rho_{34}}{1-\beta}\right) + \mathrm{Li}_2\left(1-\frac{\rho_{34}}{1+\beta}\right) + \mathcal{O}(\epsilon)\,,\end{aligned} \tag{B.3}$$

where $\beta = \sqrt{1-m_t^2/E_4^2}$ and $\rho_{ij} = p_i\cdot p_j/(E_iE_j)$. To simplify the discussion, it is convenient to define a function I_Ω that contains all the information about integration over angles of the emitted gluon. We write

$$\begin{aligned}g_{s,b}^2\int[\mathrm{d}p_k]\,\frac{p_i\cdot p_j}{(p_i\cdot p_k)\,(p_j\cdot p_k)} &= \frac{\alpha_s}{2\pi}\left(\frac{2E_{\max}}{\mu}\right)^{-2\epsilon}\frac{e^{\epsilon\gamma_E}\Gamma(1-\epsilon)}{\Gamma(1-2\epsilon)}\left(-\frac{1}{2\epsilon}\right) \\ &\quad\times\int \mathrm{d}\cos\theta\,\frac{\mathrm{d}\phi}{\pi}(\sin\theta\sin\phi)^{-2\epsilon}\,\frac{\hat{p}_i\cdot\hat{p}_4}{\hat{p}_i\cdot\hat{p}_k\,\hat{p}_4\cdot\hat{p}_k} \\ &= \frac{\alpha_s}{2\pi}\left(\frac{2E_{\max}}{\mu}\right)^{-2\epsilon}\frac{e^{\epsilon\gamma_E}\Gamma(1-\epsilon)}{\Gamma(1-2\epsilon)}\left(-\frac{1}{2\epsilon}\right)\,I_\Omega,\end{aligned} \tag{B.4}$$

where $\hat{p} = p/E_p$. We present the results for the functions I_Ω for the three relevant cases below.

B.1 One massive and one massless emitter — arbitrary angle

We consider the case when one emitter is massless, $p_i^2 = 0$, and the other is massive, $p_4^2 = m_t^2$. The function I_Ω reads

$$I_\Omega = -\frac{1}{\epsilon} + \mathcal{I}^{(0)} + \epsilon\,\mathcal{I}^{(1)} + \mathcal{O}\left(\epsilon^2\right)\,, \tag{B.5}$$

where the different terms reads

$$\begin{aligned}\mathcal{I}^{(0)} &= 2\log\left(\frac{E_4\,\rho_{i4}}{m_t}\right),\\ \mathcal{I}^{(1)} &= -2\Bigg[\frac{1}{4}\log^2\left(\frac{1-\beta}{1+\beta}\right)+\log\left(\frac{\rho_{i4}}{1+\beta}\right)\log\left(\frac{\rho_{i4}}{1-\beta}\right)\\ &\qquad+\mathrm{Li}_2\left(1-\frac{\rho_{i4}}{1+\beta}\right)+\mathrm{Li}_2\left(1-\frac{\rho_{i4}}{1-\beta}\right)\Bigg].\end{aligned} \tag{B.6}$$

The explicit expressions for $\mathcal{I}^{(0)}$ and $\mathcal{I}^{(1)}$ agree with the results in ref. [58].

B.2 One massive and one massless emitter — back-to-back kinematics

The previous result simplifies when the two emitters are back-to-back. We consider the case of one massless and one massive emitter, $p_i^2 = 0$ and $p_4^2 = m_t^2$, in the case when $\vec{p}_i + \vec{p}_4 = 0$. The function I_Ω reads

$$I_\Omega = 2^{-4\epsilon}\,B\left(\frac{1}{2}-\epsilon,\frac{1}{2}-\epsilon\right) \tag{B.7}$$

$$\times\left[B\left(-\epsilon,1-\epsilon\right)+\frac{2\beta}{1+\beta}\frac{\Gamma^2\left(1-\epsilon\right)}{\Gamma\left(2-2\epsilon\right)}\,{}_2F_1\left(1,1-\epsilon,2-2\epsilon,\frac{2\beta}{1+\beta}\right)\right]. \tag{B.8}$$

B.3 Two massless emitters — arbitrary angles

When the two emitters are massless, the result reads (see e.g. ref. [41])

$$I_\Omega = -\frac{1}{\epsilon}\,\rho_{ij}\,{}_2F_1\left(1,1,1-\epsilon,1-\frac{\rho_{ij}}{2}\right). \tag{B.9}$$

References

[1] P. Nason, S. Dawson and R.K. Ellis, *The Total Cross-Section for the Production of Heavy Quarks in Hadronic Collisions*, *Nucl. Phys. B* **303** (1988) 607 [INSPIRE].

[2] J.H. Kühn, A. Scharf and P. Uwer, *Electroweak corrections to top-quark pair production in quark-antiquark annihilation*, *Eur. Phys. J. C* **45** (2006) 139 [hep-ph/0508092] [INSPIRE].

[3] R. Bonciani, S. Catani, M.L. Mangano and P. Nason, *NLL resummation of the heavy quark hadroproduction cross-section*, *Nucl. Phys. B* **529** (1998) 424 [*Erratum ibid.* **803** (2008) 234] [hep-ph/9801375] [INSPIRE].

[4] S. Catani, M.L. Mangano, P. Nason and L. Trentadue, *The Top cross-section in hadronic collisions*, *Phys. Lett. B* **378** (1996) 329 [hep-ph/9602208] [INSPIRE].

[5] M. Beneke, P. Falgari and C. Schwinn, *Soft radiation in heavy-particle pair production: All-order colour structure and two-loop anomalous dimension*, *Nucl. Phys. B* **828** (2010) 69 [arXiv:0907.1443] [INSPIRE].

JHEP06(2022)061

[6] M. Czakon, A. Mitov and G.F. Sterman, *Threshold Resummation for Top-Pair Hadroproduction to Next-to-Next-to-Leading Log*, *Phys. Rev. D* **80** (2009) 074017 [arXiv:0907.1790] [INSPIRE].

[7] M. Cacciari, M. Czakon, M. Mangano, A. Mitov and P. Nason, *Top-pair production at hadron colliders with next-to-next-to-leading logarithmic soft-gluon resummation*, *Phys. Lett. B* **710** (2012) 612 [arXiv:1111.5869] [INSPIRE].

[8] M. Czakon, P. Fiedler and A. Mitov, *Total Top-Quark Pair-Production Cross Section at Hadron Colliders Through $O(\alpha_S^4)$*, *Phys. Rev. Lett.* **110** (2013) 252004 [arXiv:1303.6254] [INSPIRE].

[9] M. Czakon, D. Heymes, A. Mitov, D. Pagani, I. Tsinikos and M. Zaro, *Top-pair production at the LHC through NNLO QCD and NLO EW*, *JHEP* **10** (2017) 186 [arXiv:1705.04105] [INSPIRE].

[10] A. Behring, M. Czakon, A. Mitov, A.S. Papanastasiou and R. Poncelet, *Higher order corrections to spin correlations in top quark pair production at the LHC*, *Phys. Rev. Lett.* **123** (2019) 082001 [arXiv:1901.05407] [INSPIRE].

[11] M. Czakon, A. Mitov and R. Poncelet, *NNLO QCD corrections to leptonic observables in top-quark pair production and decay*, *JHEP* **05** (2021) 212 [arXiv:2008.11133] [INSPIRE].

[12] CMS collaboration, *Measurement of the ratio $\mathcal{B}(t \to Wb)/\mathcal{B}(t \to Wq)$ in pp collisions at $\sqrt{s} = 8$ TeV*, *Phys. Lett. B* **736** (2014) 33 [arXiv:1404.2292] [INSPIRE].

[13] CMS collaboration, *Measurement of the top quark mass using single top quark events in proton-proton collisions at $\sqrt{s} = 8$ TeV*, *Eur. Phys. J. C* **77** (2017) 354 [arXiv:1703.02530] [INSPIRE].

[14] CMS collaboration, *Measurement of Top Quark Polarisation in T-Channel Single Top Quark Production*, *JHEP* **04** (2016) 073 [arXiv:1511.02138] [INSPIRE].

[15] G.L. Kane, G.A. Ladinsky and C.P. Yuan, *Using the Top Quark for Testing Standard Model Polarization and CP Predictions*, *Phys. Rev. D* **45** (1992) 124 [INSPIRE].

[16] S.D. Rindani and P. Sharma, *Probing anomalous tbW couplings in single-top production using top polarization at the Large Hadron Collider*, *JHEP* **11** (2011) 082 [arXiv:1107.2597] [INSPIRE].

[17] Q.-H. Cao, B. Yan, J.-H. Yu and C. Zhang, *A General Analysis of Wtb anomalous Couplings*, *Chin. Phys. C* **41** (2017) 063101 [arXiv:1504.03785] [INSPIRE].

[18] G.A. González-Sprinberg and J. Vidal, *The top quark right coupling in the tbW-vertex*, *Eur. Phys. J. C* **75** (2015) 615 [arXiv:1510.02153] [INSPIRE].

[19] CDF and D0 collaborations, *Tevatron Combination of Single-Top-Quark Cross Sections and Determination of the Magnitude of the Cabibbo-Kobayashi-Maskawa Matrix Element V_{tb}*, *Phys. Rev. Lett.* **115** (2015) 152003 [arXiv:1503.05027] [INSPIRE].

[20] CMS collaboration, *Measurement of the t-channel single-top-quark production cross section and of the $| V_{tb} |$ CKM matrix element in pp collisions at $\sqrt{s} = 8$ TeV*, *JHEP* **06** (2014) 090 [arXiv:1403.7366] [INSPIRE].

[21] S. Alekhin, J. Blümlein, S. Moch and R. Plačakytė, *Isospin asymmetry of quark distributions and implications for single top-quark production at the LHC*, *Phys. Rev. D* **94** (2016) 114038 [arXiv:1508.07923] [INSPIRE].

JHEP06(2022)061

[22] CMS collaboration, *Measurement of differential cross sections and charge ratios for t-channel single top quark production in proton-proton collisions at* $\sqrt{s} = 13$ *TeV*, *Eur. Phys. J. C* **80** (2020) 370 [arXiv:1907.08330] [INSPIRE].

[23] ATLAS collaboration, *Fiducial, total and differential cross-section measurements of t-channel single top-quark production in pp collisions at 8 TeV using data collected by the ATLAS detector*, *Eur. Phys. J. C* **77** (2017) 531 [arXiv:1702.02859] [INSPIRE].

[24] G. Bordes and B. van Eijk, *Calculating QCD corrections to single top production in hadronic interactions*, *Nucl. Phys. B* **435** (1995) 23 [INSPIRE].

[25] J.M. Campbell, R.K. Ellis and F. Tramontano, *Single top production and decay at next-to-leading order*, *Phys. Rev. D* **70** (2004) 094012 [hep-ph/0408158] [INSPIRE].

[26] Q.-H. Cao and C.P. Yuan, *Single top quark production and decay at next-to-leading order in hadron collision*, *Phys. Rev. D* **71** (2005) 054022 [hep-ph/0408180] [INSPIRE].

[27] Q.-H. Cao, R. Schwienhorst, J.A. Benitez, R. Brock and C.P. Yuan, *Next-to-leading order corrections to single top quark production and decay at the Tevatron: 2.* t^- *channel process*, *Phys. Rev. D* **72** (2005) 094027 [hep-ph/0504230] [INSPIRE].

[28] B.W. Harris, E. Laenen, L. Phaf, Z. Sullivan and S. Weinzierl, *The Fully Differential Single Top Quark Cross-Section in Next to Leading Order QCD*, *Phys. Rev. D* **66** (2002) 054024 [hep-ph/0207055] [INSPIRE].

[29] R. Schwienhorst, C.P. Yuan, C. Mueller and Q.-H. Cao, *Single top quark production and decay in the t-channel at next-to-leading order at the LHC*, *Phys. Rev. D* **83** (2011) 034019 [arXiv:1012.5132] [INSPIRE].

[30] M. Brucherseifer, F. Caola and K. Melnikov, *On the NNLO QCD corrections to single-top production at the LHC*, *Phys. Lett. B* **736** (2014) 58 [arXiv:1404.7116] [INSPIRE].

[31] E.L. Berger, J. Gao, C.P. Yuan and H.X. Zhu, *NNLO QCD Corrections to t-channel Single Top-Quark Production and Decay*, *Phys. Rev. D* **94** (2016) 071501 [arXiv:1606.08463] [INSPIRE].

[32] E.L. Berger, J. Gao and H.X. Zhu, *Differential Distributions for t-channel Single Top-Quark Production and Decay at Next-to-Next-to-Leading Order in QCD*, *JHEP* **11** (2017) 158 [arXiv:1708.09405] [INSPIRE].

[33] J. Campbell, T. Neumann and Z. Sullivan, *Single-top-quark production in the t-channel at NNLO*, *JHEP* **02** (2021) 040 [arXiv:2012.01574] [INSPIRE].

[34] Q.-H. Cao, P. Sun, B. Yan, C.P. Yuan and F. Yuan, *Transverse Momentum Resummation for t-channel single top quark production at the LHC*, *Phys. Rev. D* **98** (2018) 054032 [arXiv:1801.09656] [INSPIRE].

[35] R. Frederix, D. Pagani and I. Tsinikos, *Precise predictions for single-top production: the impact of EW corrections and QCD shower on the t-channel signature*, *JHEP* **09** (2019) 122 [arXiv:1907.12586] [INSPIRE].

[36] T. Liu, K. Melnikov and A.A. Penin, *Nonfactorizable QCD Effects in Higgs Boson Production via Vector Boson Fusion*, *Phys. Rev. Lett.* **123** (2019) 122002 [arXiv:1906.10899] [INSPIRE].

[37] R.J. Glauber, *Lectures in Theoretical Physics*, Wiley-Interscience, New York, U.S.A. (1959).

[38] H. Cheng and T.T. Wu, *Impact factor and exponentiation in high-energy scattering processes*, *Phys. Rev.* **186** (1969) 1611 [INSPIRE].

JHEP06(2022)061

[39] C. Brønnum-Hansen, K. Melnikov, J. Quarroz and C.-Y. Wang, *On non-factorisable contributions to t-channel single-top production*, *JHEP* **11** (2021) 130 [arXiv:2108.09222] [INSPIRE].

[40] S. Catani and M.H. Seymour, *A general algorithm for calculating jet cross-sections in NLO QCD*, *Nucl. Phys. B* **485** (1997) 291 [*Erratum ibid.* **510** (1998) 503] [hep-ph/9605323] [INSPIRE].

[41] F. Caola, K. Melnikov and R. Röntsch, *Nested soft-collinear subtractions in NNLO QCD computations*, *Eur. Phys. J. C* **77** (2017) 248 [arXiv:1702.01352] [INSPIRE].

[42] P. Nogueira, *Automatic Feynman graph generation*, *J. Comput. Phys.* **105** (1993) 279.

[43] J. Kuipers, T. Ueda, J.A.M. Vermaseren and J. Vollinga, *FORM version 4.0*, *Comput. Phys. Commun.* **184** (2013) 1453 [arXiv:1203.6543] [INSPIRE].

[44] B. Ruijl, T. Ueda and J. Vermaseren, *FORM version 4.2*, arXiv:1707.06453 [INSPIRE].

[45] M.L. Mangano and S.J. Parke, *Multiparton amplitudes in gauge theories*, *Phys. Rept.* **200** (1991) 301 [hep-th/0509223] [INSPIRE].

[46] R. Kleiss and W.J. Stirling, *Spinor Techniques for Calculating $p\bar{p} \to W^{\pm}/Z^0+$ Jets*, *Nucl. Phys. B* **262** (1985) 235 [INSPIRE].

[47] J. Alwall et al., *The automated computation of tree-level and next-to-leading order differential cross sections, and their matching to parton shower simulations*, *JHEP* **07** (2014) 079 [arXiv:1405.0301] [INSPIRE].

[48] R.K. Ellis and G. Zanderighi, *Scalar one-loop integrals for QCD*, *JHEP* **02** (2008) 002 [arXiv:0712.1851] [INSPIRE].

[49] S. Carrazza, R.K. Ellis and G. Zanderighi, *QCDLoop: a comprehensive framework for one-loop scalar integrals*, *Comput. Phys. Commun.* **209** (2016) 134 [arXiv:1605.03181] [INSPIRE].

[50] G. Cullen, M. Koch-Janusz and T. Reiter, *Spinney: A Form Library for Helicity Spinors*, *Comput. Phys. Commun.* **182** (2011) 2368 [arXiv:1008.0803] [INSPIRE].

[51] W.L. van Neerven and J.A.M. Vermaseren, *Large loop integrals*, *Phys. Lett. B* **137** (1984) 241 [INSPIRE].

[52] Z. Bern, L.J. Dixon, D.C. Dunbar and D.A. Kosower, *Fusing gauge theory tree amplitudes into loop amplitudes*, *Nucl. Phys. B* **435** (1995) 59 [hep-ph/9409265] [INSPIRE].

[53] Z. Bern, L.J. Dixon and D.A. Kosower, *Dimensionally regulated one loop integrals*, *Phys. Lett. B* **302** (1993) 299 [*Erratum ibid.* **318** (1993) 649] [hep-ph/9212308] [INSPIRE].

[54] G. Passarino and M.J.G. Veltman, *One Loop Corrections for e^+e^- Annihilation Into $\mu^+\mu^-$ in the Weinberg Model*, *Nucl. Phys. B* **160** (1979) 151 [INSPIRE].

[55] S. Badger, G. Mogull and T. Peraro, *Local integrands for two-loop all-plus Yang-Mills amplitudes*, *JHEP* **08** (2016) 063 [arXiv:1606.02244] [INSPIRE].

[56] S.D. Ellis and D.E. Soper, *Successive combination jet algorithm for hadron collisions*, *Phys. Rev. D* **48** (1993) 3160 [hep-ph/9305266] [INSPIRE].

[57] J. Ellis, *TikZ-Feynman: Feynman diagrams with TikZ*, *Comput. Phys. Commun.* **210** (2017) 103 [arXiv:1601.05437] [INSPIRE].

[58] S. Alioli, P. Nason, C. Oleari and E. Re, *A general framework for implementing NLO calculations in shower Monte Carlo programs: the POWHEG BOX*, *JHEP* **06** (2010) 043 [arXiv:1002.2581] [INSPIRE].

JHEP06(2022)061